Latest result of geoneutrino measurement with KamLAND

Research Center for Neutrino Science, Tohoku University, Japan
Nanami Kawada

The 29th International Workshop on Weak Interaction and Neutrinos (WIN2023)

We are the KamLAND collaboration !!

>50 researchers from US, Netherlands and Japan

TOHOKU UNIVERSITY
東京大学 THE UNIVERSITY OF TOKYO
大阪大学 OSAKA UNIVERSITY
VIRGINIA TECH
BERKELEY LAB
THE UNIVERSITY OF TENNESSEE KNOXVILLE
BOSTON UNIVERSITY
Nikhef
TUNL
UNIVERSITY of HAWAIʻI
TOKUSHIMA UNIVERSITY

Contents

- Neutrino geoscience
- The KamLAND experiment
- Latest result of geoneutrino measurement

Contents

- Neutrino geoscience
- The KamLAND experiment
- Latest result of geoneutrino measurement

What formed our planet ?

Credit: Getty Images/iStockphoto

Traditional geoscientific approaches

Seismology

Structual modeling by earthquake analysis
"Core—mantle—crust" layers in the Earth

Geochemistry / Cosmochemistry

Compositional estimation based on rock samples and chondrite meteorites

Geothermology

Heat flux measurement at the surface

etc…

Open questions

Which type of meteorites formed the Earth?
What powers the geodynamics?
How much layers the mantle have?

Geoneutrino is a key of these questions.

"Neutrino geoscience"

Geothermal evolution and geodynamics

©National geographic

©全日本防災計画協会

Ref : Arevalo et al. 2009

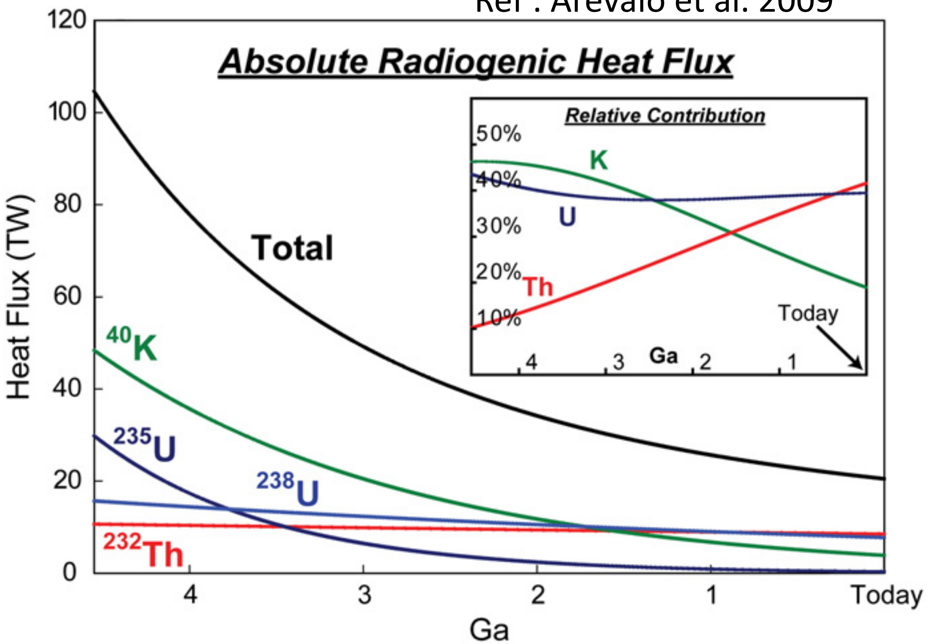

Earth heat budget

The history of the Earth is a global cooling process.
The geodynamics are powered by heat inside the Earth.

Understanding the heat amount and its source inside the Earth is quite important.

Surface heat flux measurements

Bore-hole heat measurements
Total heat flux is 47±2 TW.
Source : primordial heat + radiogenic heat

? **The breakdown is unknown.**

Radiogenic heat

Heat generated by radioactive elements
Past amount is calculated from the present value.

? **Important for understanding the geothermal evolution**
Different prediction from geophysics and geochemistry

→ Direct measurement is necessary.

Motivation of geoneutrino observation

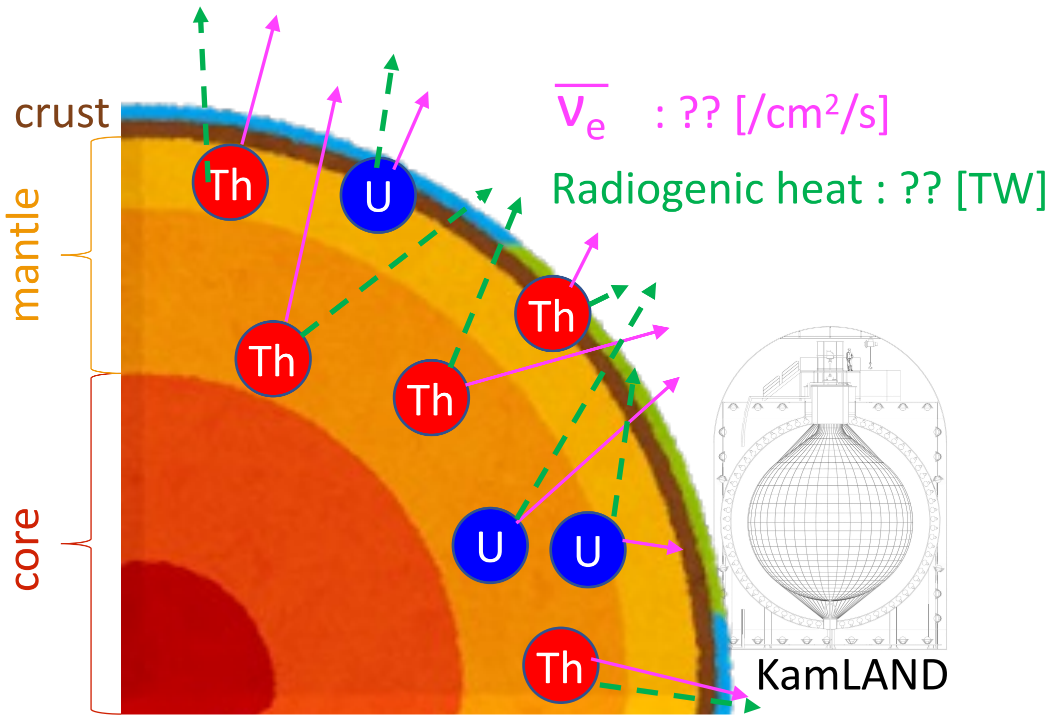

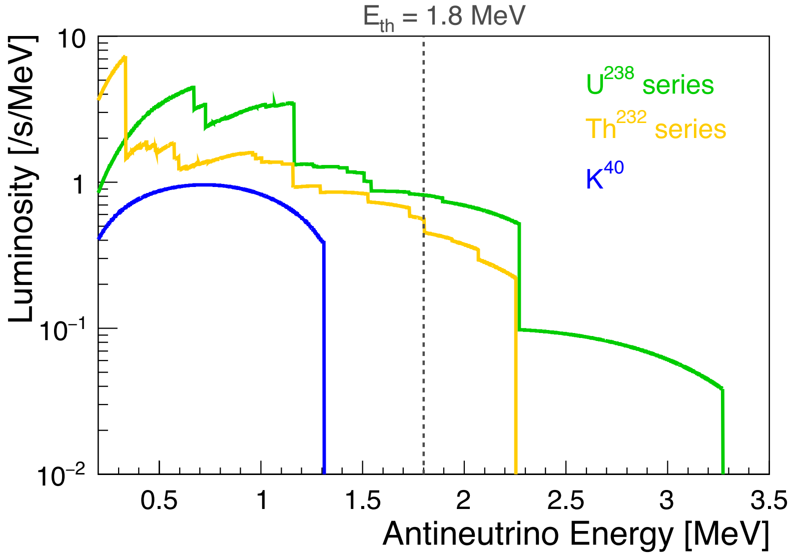

Emission of $\overline{\nu}_e$ from U, Th and K.

$$^{238}\mathrm{U} \rightarrow {}^{206}\mathrm{Pb} + 8\alpha + 6\mathrm{e}^- + 6\overline{\nu}_\mathrm{e} + 51.7\ \mathrm{MeV}$$

$$^{232}\mathrm{Th} \rightarrow {}^{208}\mathrm{Pb} + 6\alpha + 4\mathrm{e}^- + 4\overline{\nu}_\mathrm{e} + 42.7\ \mathrm{MeV}$$

$$^{40}\mathrm{K} \rightarrow {}^{40}\mathrm{Ca} + \mathrm{e}^- + \overline{\nu}_\mathrm{e} + 1.311\ \mathrm{MeV}$$

Geoneutrino total flux

$\overline{\nu}_e$ flux $\propto$ U, Th $\propto$ Radiogenic heat

Test of Earth's heat budget

Geoneutrino spectrum

U and Th have different $\overline{\nu}_e$ energy.

Test of Earth's chemical composition

Contents

The KamLAND detector

Detector site and components

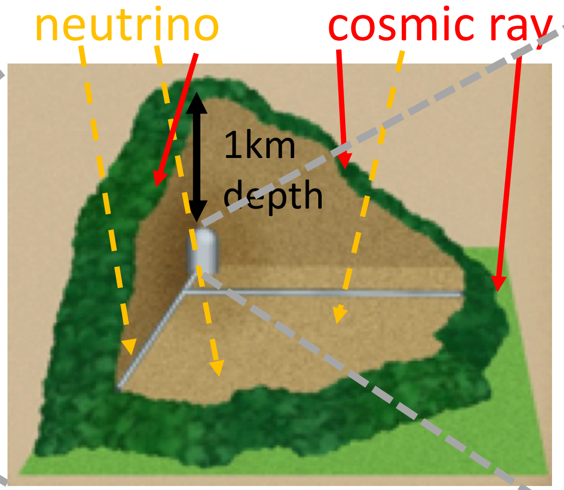

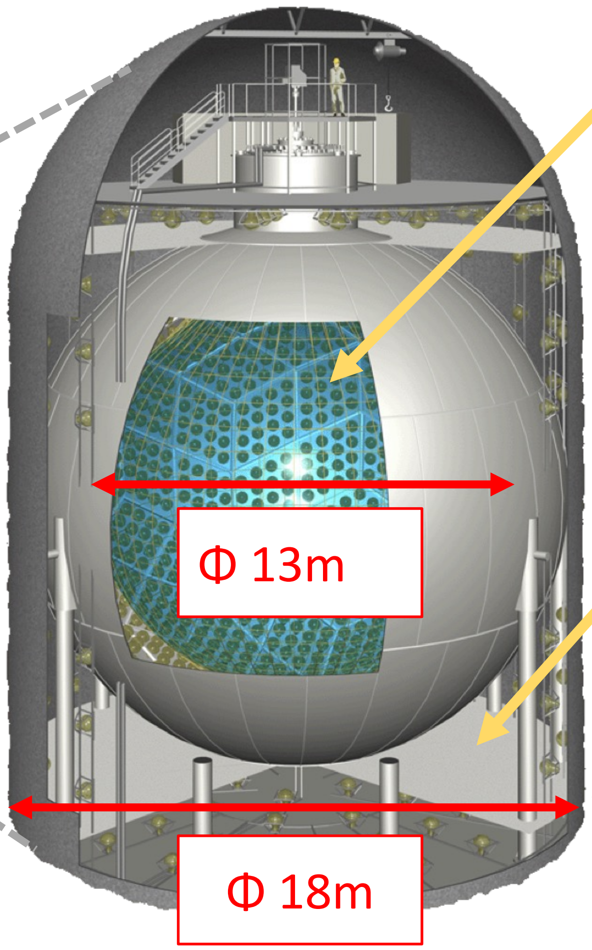

Scintillation inner detector

1kt purified liquid scintillator
(PC+Dodecane+PPO mixture)
1325 17" + 554 20" PMTs
photo coverage 34%
Neutrino detection

Water Cherenkov outer detector

3.2 kt purified water
225(140) 20" PMTs
passive shielding
active veto to muon

Neutrino detection channel

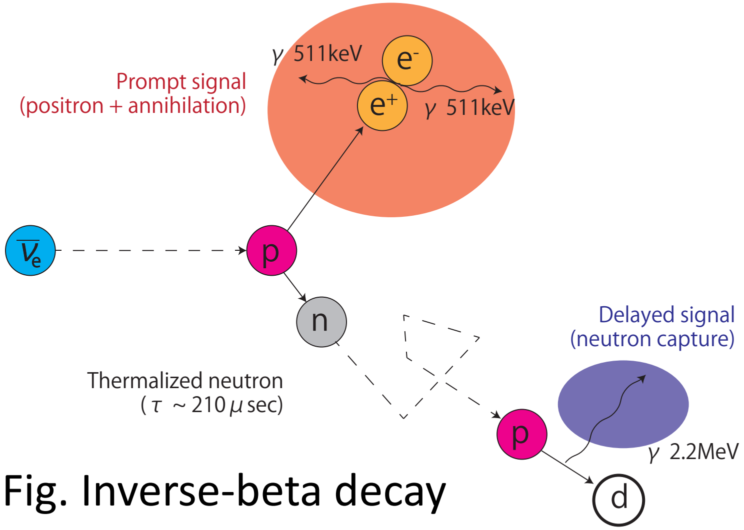

Fig. Inverse-beta decay

Anti-electron neutrino detection by inverse-beta decay

- ✓ Significant background reduction by two-fold coincidence
- ✓ Neutrino energy reconstruction from prompt scintillation
- ✗ No directional information → reactor neutrinos are background

History of neutrino geoscience in KamLAND

2002 Beginning of KamLAND

2005 Nature 436, 499–503

2011 Nature Geoscience 4, 467–651

2022 Geophysical Research Letters Volume 49, Issue 16, e2022GL099566

First evidence of geoneutrino detection

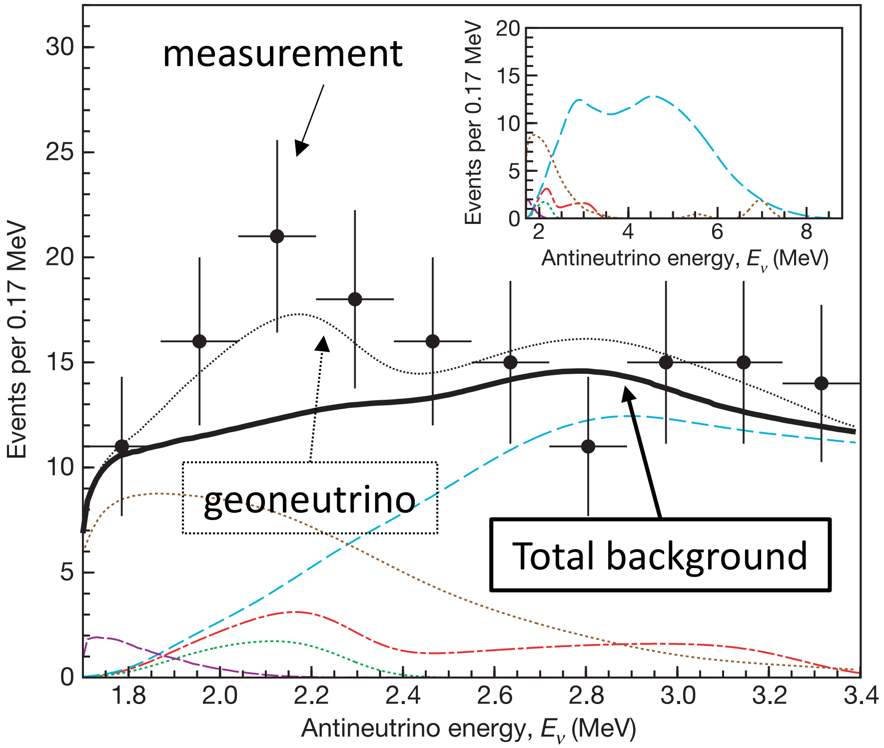

$28.0^{+15.6}_{-14.6}$ events (56% error)

749 days, 0.71×10^{32} proton-year

"The beginning of neutrino geoscience"

History of neutrino geoscience in KamLAND

2002 Beginning of KamLAND

2005 Nature 436, 499–503

2011 Nature Geoscience 4, 467–651

2022 Geophysical Research Letters
Volume 49, Issue 16,
e2022GL099566

First evidence of "partial radiogenic Earth"

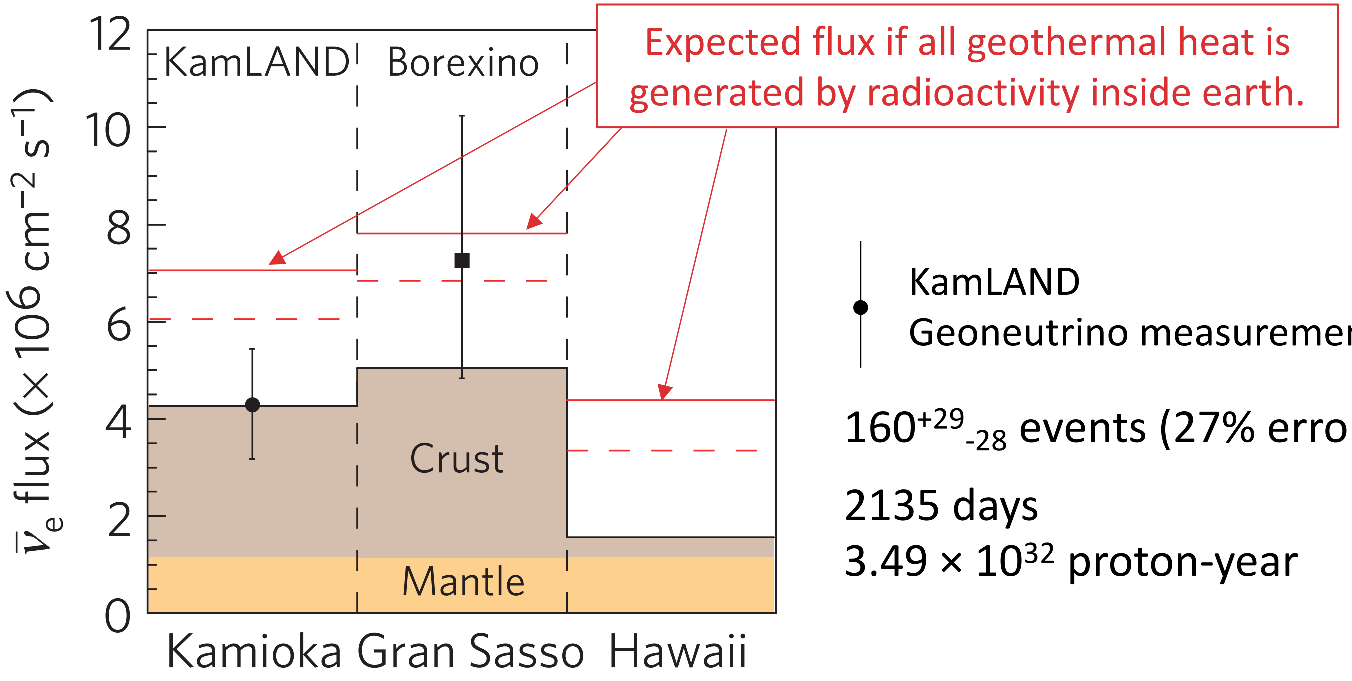

KamLAND Geoneutrino measurement

160^{+29}_{-28} events (27% error)

2135 days

3.49×10^{32} proton-year

This result implies radiogenic heat inside the Earth is less than total heat flow at the surface.

There is residual primordial heat inside the Earth.
Our planet is cooling.

History of neutrino geoscience in KamLAND

2002 Beginning of KamLAND

2005 Nature 436, 499–503

2011 Nature Geoscience 4, 467–651

2022 Geophysical Research Letters Volume 49, Issue 16, e2022GL099566

Reactor-off period in Japan

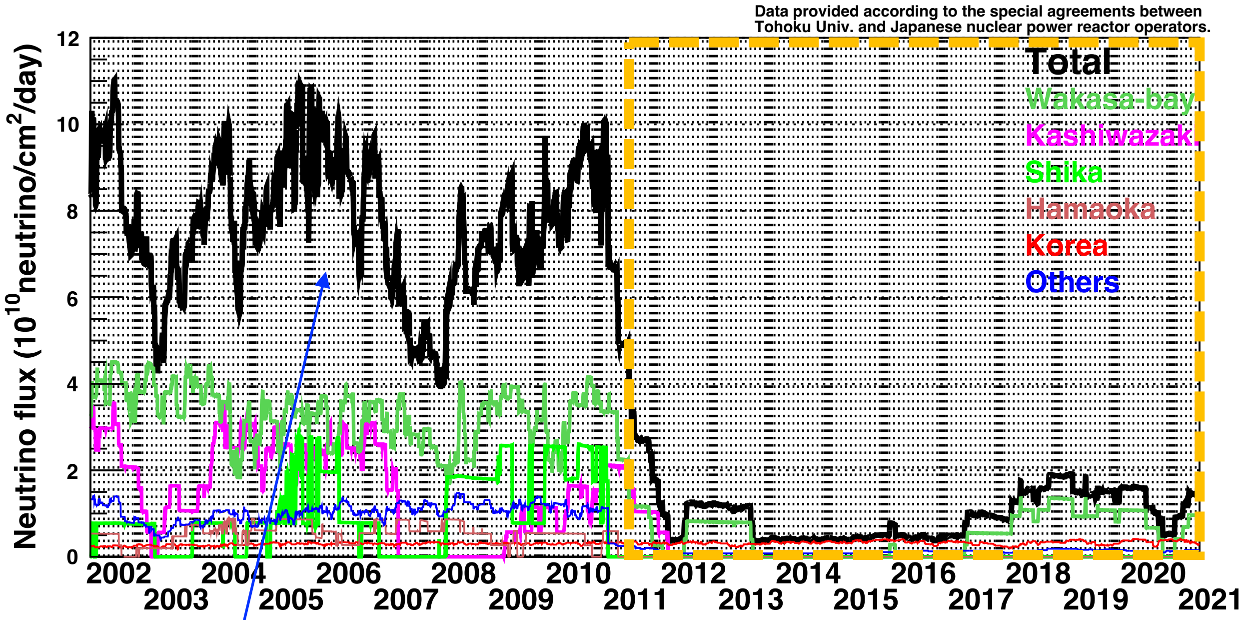

Reactor neutrino is the dominant background of geoneutrino signals.

Most of Japanese reactors have been shut down due to the 3.11 earthquake in 2011.

This "reactor-off" period gives us large signal-to-noise ratio of geoneutrino observation.

History of neutrino geoscience in KamLAND

- 2002 Beginning of KamLAND
- 2005 Nature 436, 499–503
- 2011 Nature Geoscience 4, 467–651
- 2022 Geophysical Research Letters Volume 49, Issue 16, e2022GL099566

First result of measurement in low-reactor period

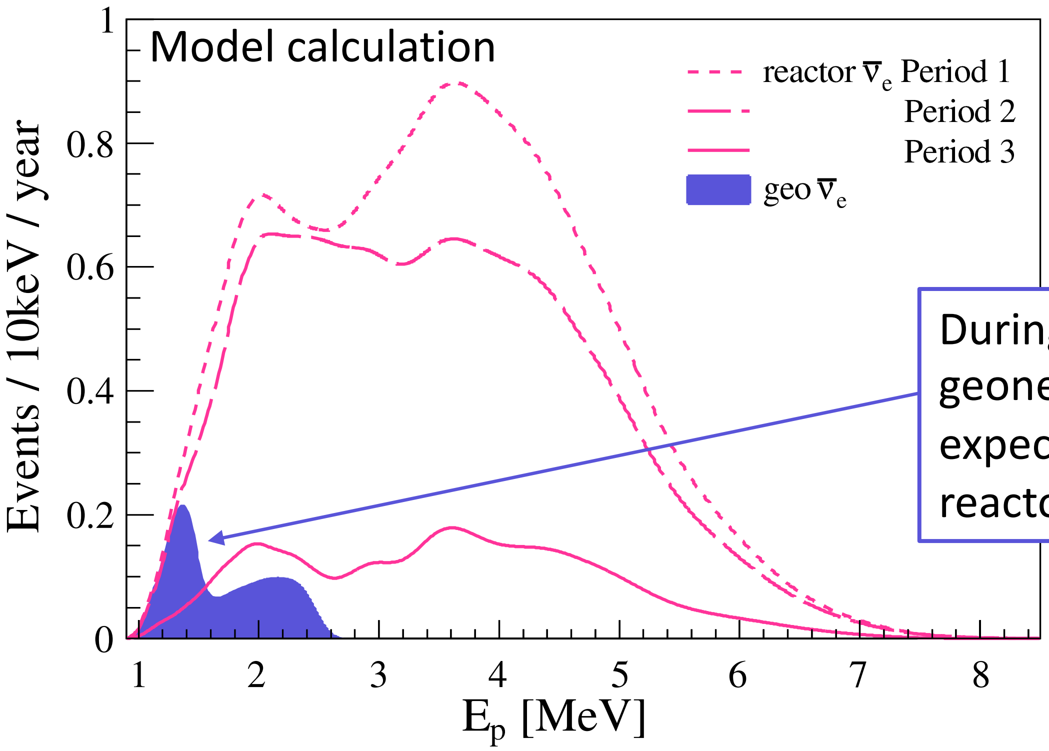

During low-reactor period, geoneutrino spectrum was expected to appear above the reactor neutrino spectrum.

Reactor off period significantly improved observation accuracy.

Contents

- Neutrino geoscience
- The KamLAND experiment
- Latest result of geoneutrino measurement

Best fit geoneutrino signals

Best-fit time variation

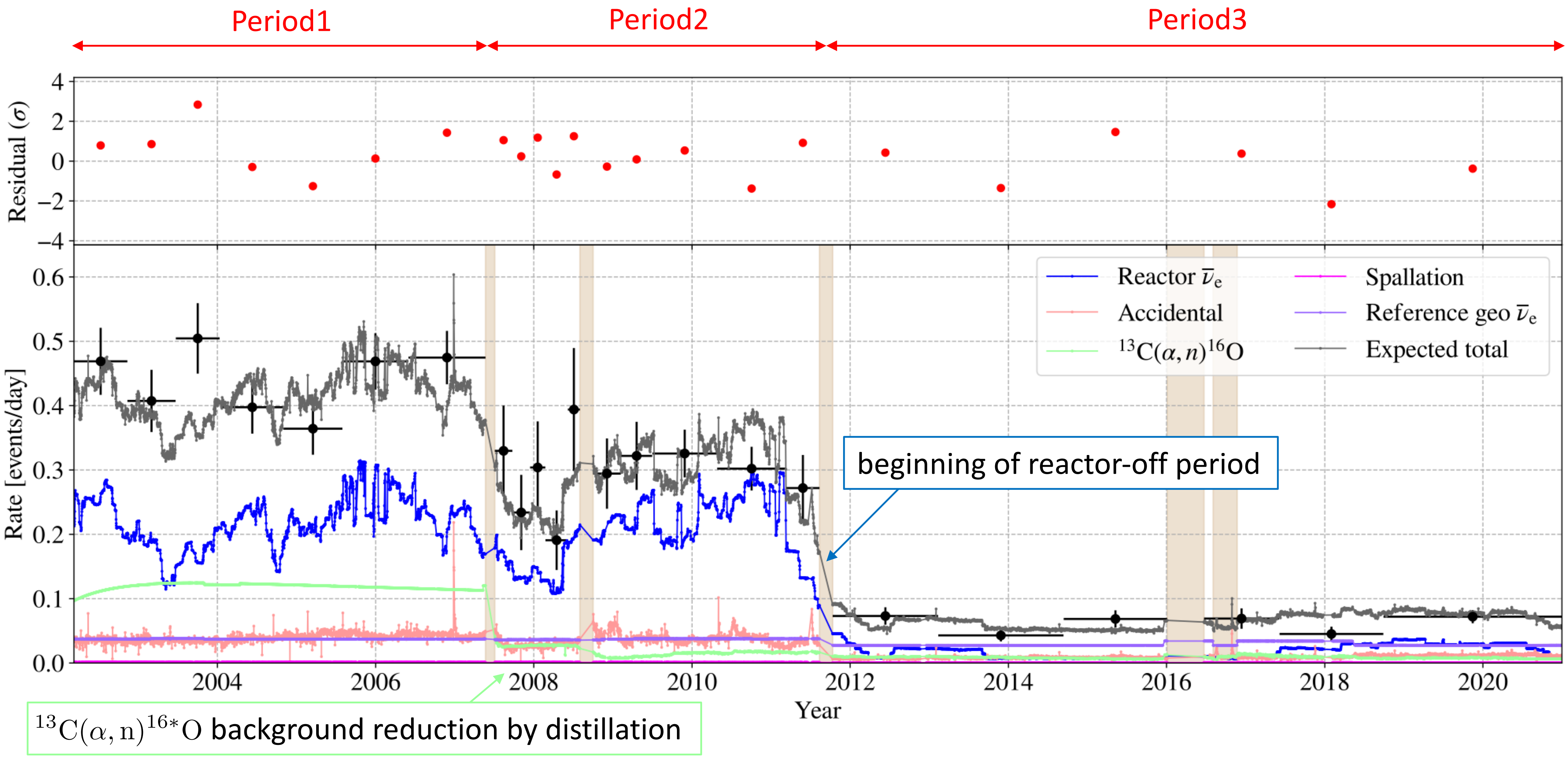

Best fit geoneutrino signals

Rate + Shape + Time un-binned likelihood

Energy : 0.9 ≤ (Prompt Energy) ≤ 8.5 [MeV], 72 bins

Time : each KamLAND run (~24 hour bin)

scan parameter : geo $\overline{\nu}_e$ signal (U,Th)

fit parameter : $\Delta m_{21}{}^2$, θ_{12}, θ_{13}, backgrounds, systematics

Simultaneous scan of the oscillation parameters and geoneutrinos

Table. Best fit geoneutrino signals and backgrounds

	Period1	Period2	Period3	All Period
energy range [MeV]	0.9–2.6	0.9–2.6	0.9–2.6	0.9–2.6
live time [day]	1485.5	1151.5	2590.0	5227.0
Reactor $\overline{\nu}_e$	325.75	229.64	48.97	604.36
$^{13}C(\alpha,n)^{16}O$	177.66	20.42	22.18	222.26
Accidental	59.35	40.53	24.79	124.67
Spallation ($^8He/^9Li$)	1.52	1.05	1.69	4.26
Background total	620.21	334.07	171.98	1126.26
observed	651	363	164	1178

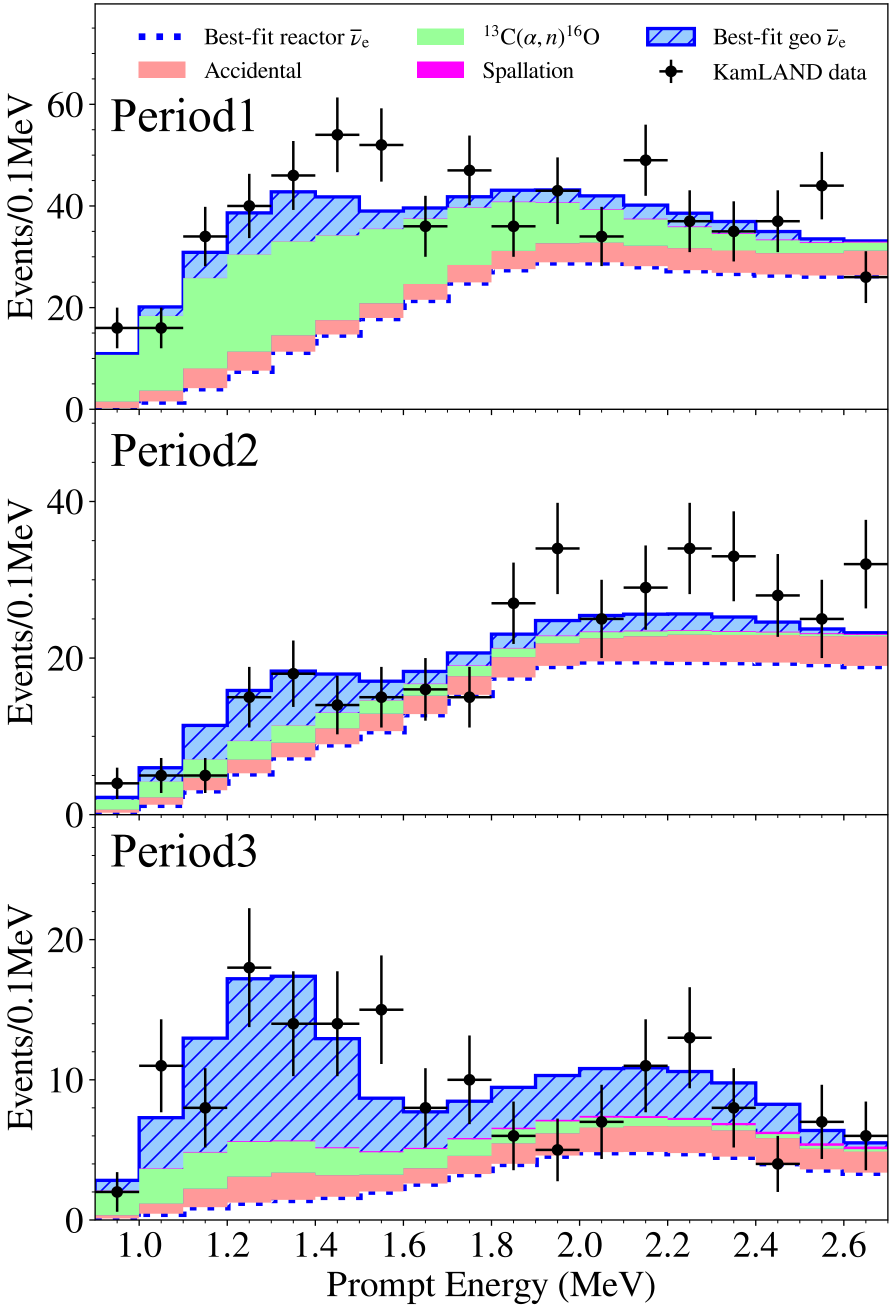

Geoneutrino flux measured by KamLAND

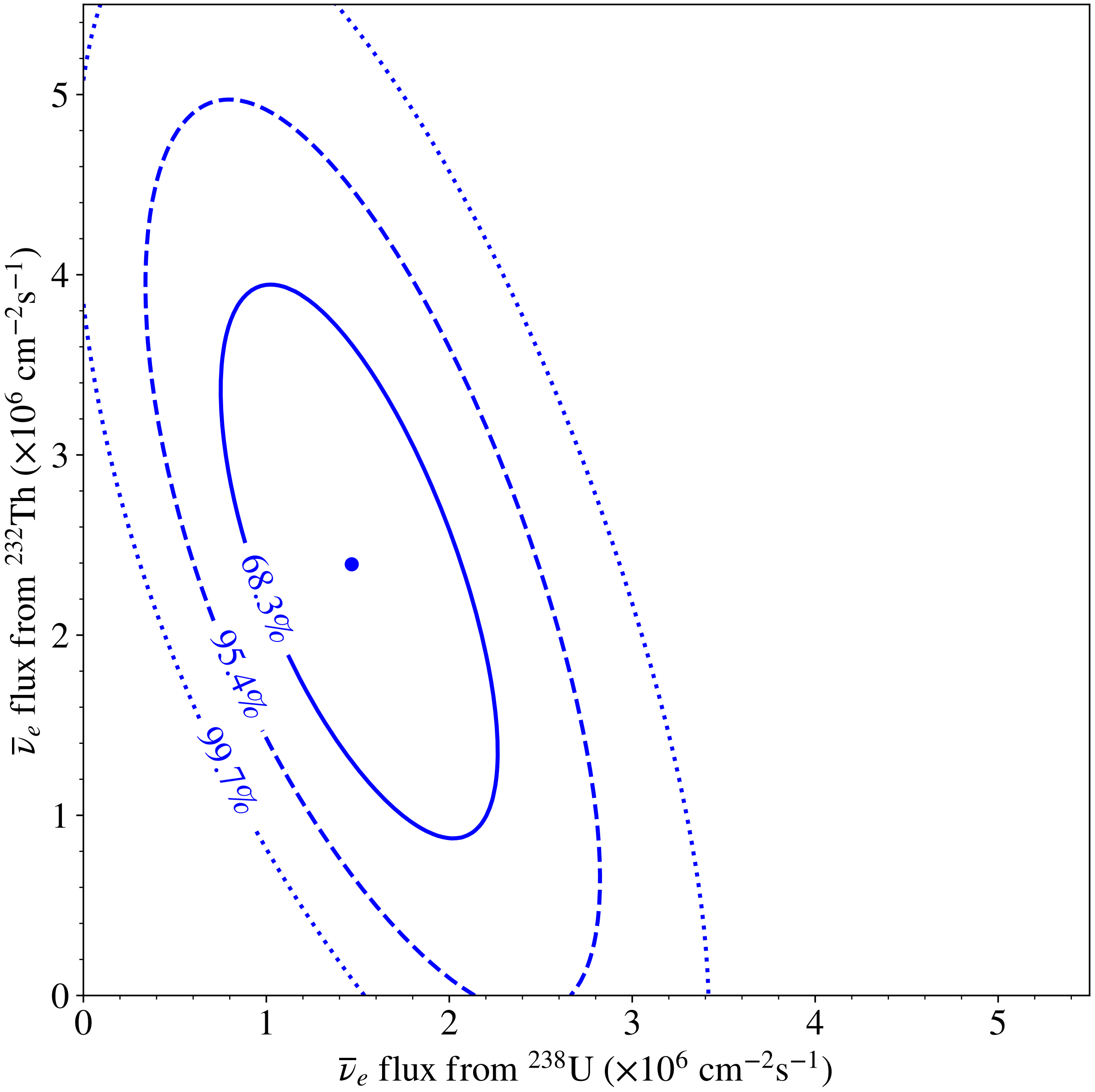

Best fit geoneutrino signals

	$N_{\mathrm{U/Th}}$ [event]	flux [$\times 10^5$ cm^{-2}s^{-1}]	flux [TNU]	0-signal rejection
U	$116.6^{+41.0}_{-38.5}$	$14.7^{+5.2}_{-4.8}$	$19.1^{+6.7}_{-6.3}$	3.343σ
Th	$57.5^{+24.5}_{-24.1}$	$23.9^{+10.2}_{-10.0}$	$9.7^{+4.1}_{-4.1}$	2.386σ
U + Th	$173.7^{+29.2}_{-27.7}$	$32.1^{+5.8}_{-5.3}$	$28.6^{+5.1}_{-4.8}$	8.3σ

KamLAND detected significant geoneutrino signal from both uranium and thorium inside the Earth.

Spectroscopic measurement of geoneutrinos from uranium and thorium was achieved.

Radiogenic heat measurement by KamLAND

KamLAND result

Crust estimation

central value : Enomoto 2007
uncertainty : Rudnick&Gao 2014
Th/U ratio : Wipperfurth et al 2018

Radiogenic heat from mantle

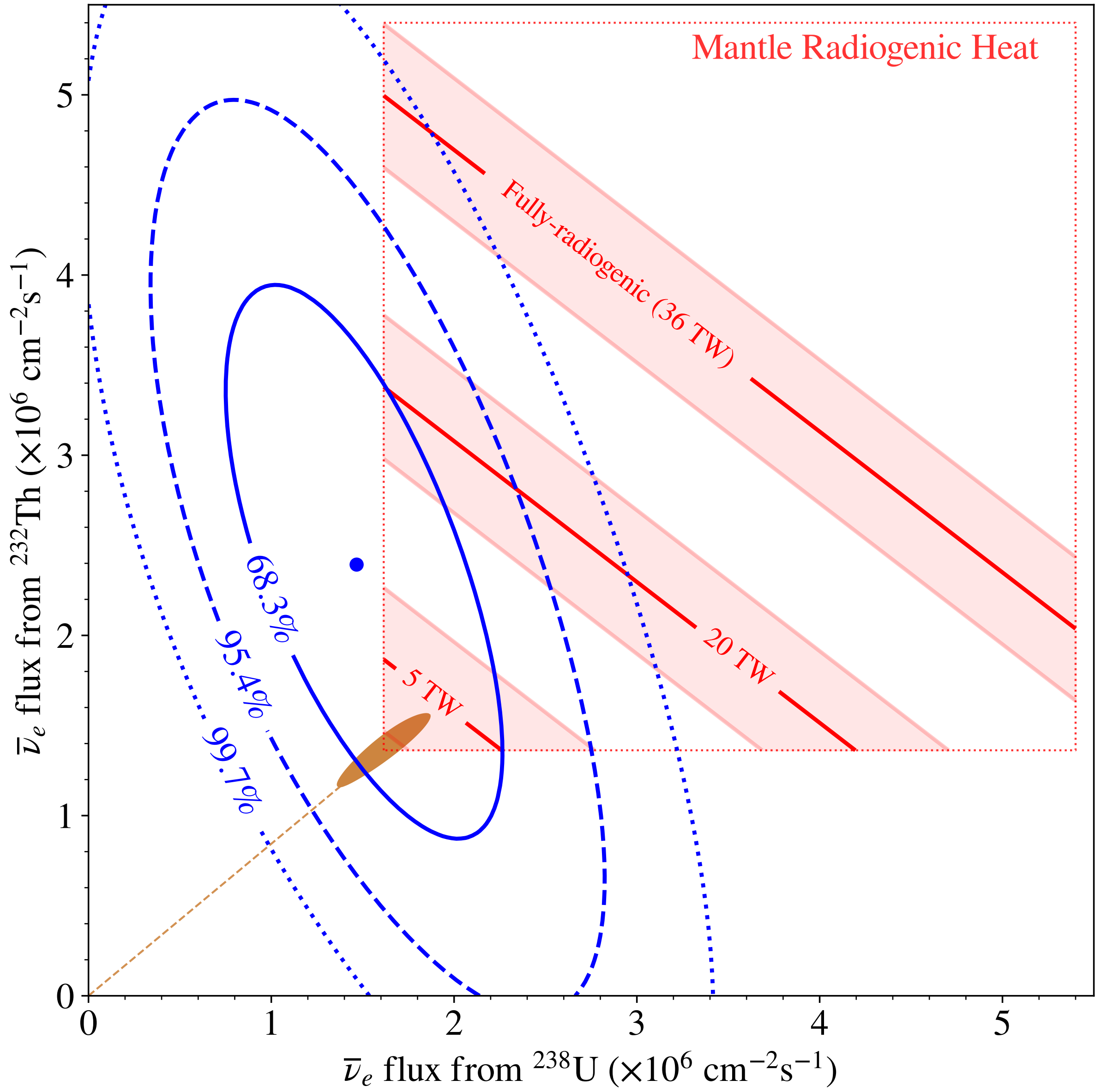

Conversion coefficients between flux and radiogenic heat in homogeneous mantle

$$Q^{U,Th}_{mantle} = (\Phi^{U,Th} - \Phi^{U,Th}_{crust}) \frac{dQ^{U,Th}_{mantle}}{d\Phi^{U,Th}_{mantle}}$$

measured flux at the surface — flux estimate in crustal model

Adding heat estimate from crust, ^{238}U : 3.4 TW, ^{232}Th : 3.6 TW

$$Q^{U} = 3.3^{+3.2}_{-0.8}\ \mathrm{TW}$$
$$Q^{Th} = 12.1^{+8.3}_{-8.6}\ \mathrm{TW}$$
$$Q^{U} + Q^{Th} = 15.4^{+8.3}_{-7.9}\ \mathrm{TW}$$

Convective Uray ratio = $0.13^{+0.15}_{-0.06}$

Heat contribution separately from U and Th has been measured.

Comparison to Earth models

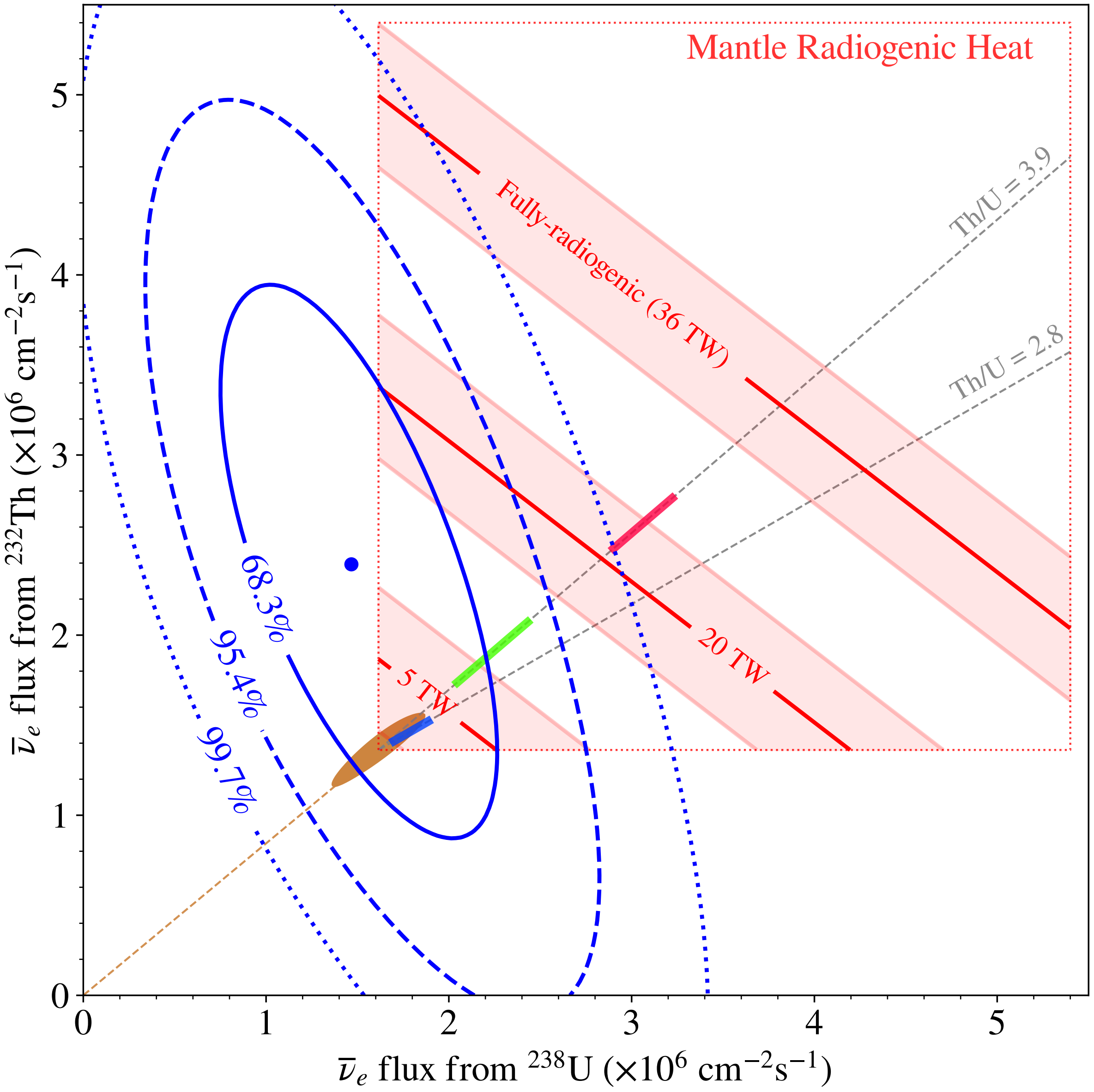

BSE models (Sramek et al 2013)

Low-Q (10-15 TW) Based on compositional analysis of enstatite chondrites and isotopic constraints (U : 12±2 ppb, Th : 43±4 ppb)

Middle-Q (17-22 TW) Based on compositional analysis of CI carbonaceous chondrites and earth samples (U : 20±4 ppb, Th : 80±13 ppb)

Consistent with the KamLAND data.

High-Q (>25 TW) Based on balancing mantle viscosity and heat dissipation. Predicting relatively large amount of radiogenic heat for mantle convection. (U : 35±4 ppb, Th : 140±14 ppb)

Inconsistent with the KamLAND data

Comparison to Earth models

Tension between KamLAND data and models

$$\chi^2_{\min} = \min_{(\alpha^{U}_{crust}, \alpha^{Th}_{crust}, \alpha_{BSE})} \left\{ \chi^2_{KL}(\Phi^{U}_{crust} + \Phi^{Th}_{crust} + \Phi_{mantle}) + \chi^2_{penalty} \right\}$$

$$\Phi_{mantle} = (Q_{BSE} - Q^{U}_{crust} - Q^{Th}_{crust}) \frac{d\Phi^{U,Th}_{mantle}}{dQ^{U,Th}_{mantle}}$$

$$\chi^2_{penalty} = (\alpha^{U}_{crust})^2 + (\alpha^{Th}_{crust})^2 + (\alpha^{Th/U}_{crust})^2 + (\alpha_{BSE})^2$$

Constraints from crust and BSE models

$$\alpha^{U}_{crust} = \frac{Q^{U}_{crust} - Q^{U,Model}_{crust}}{Q^{U,Model}_{crust} \times (24\%)} = \frac{\Phi^{U}_{crust} - \Phi^{U,Model}_{crust}}{\Phi^{U,Model}_{crust} \times (24\%)}$$

$$\alpha^{Th}_{crust} = \frac{Q^{Th}_{crust} - Q^{Th,Model}_{crust}}{Q^{Th,Model}_{crust} \times (11\%)} = \frac{\Phi^{Th}_{crust} - \Phi^{Th,Model}_{crust}}{\Phi^{Th,Model}_{crust} \times (11\%)}$$

$$\alpha^{Th/U}_{crust} = \frac{\alpha^{Th}_{crust} - \alpha^{U}_{crust}}{\alpha^{U}_{crust} \times \binom{4.8\%}{3.5\%}} \quad (\because \text{Th/U mass ratio} = 3.95^{+0.19}_{-0.13})$$

$$\alpha_{BSE} = \frac{Q_{BSE} - Q^{Model}_{BSE}}{Q^{Model}_{BSE} \times (10\%)} \qquad Q^{Model}_{BSE} = 28.2\,\text{TW} \qquad \text{(High-Q model)}$$

	Q^{Model}_{crust} [TW]	Φ^{Model}_{crust} [10^5 cm^{-2}s^{-1}]	$\frac{dQ_{mantle}}{d\Phi_{mantle}}$ [10^{-5} TW/cm^{-2}s^{-1}]
^{238}U	3.35	17.19	7.28
^{232}Th	3.61	14.51	9.32

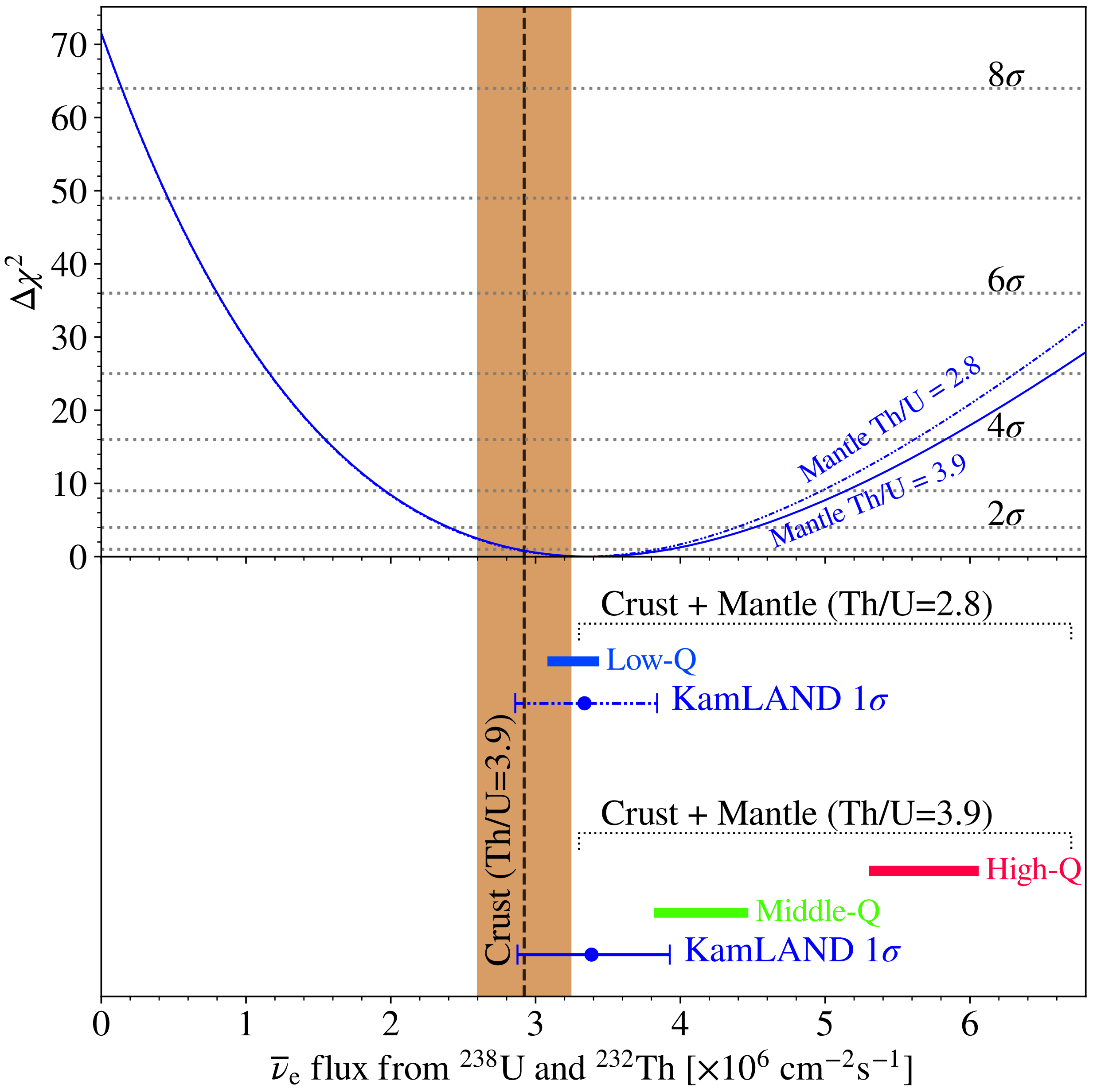

Comparison to Earth models

Assuming homogeneous mantle composition,

High-Q model is disfavored at 99.76%.

Assuming U and Th concentration at the mantle-core boundary,

High-Q model is disfavored at 97.9%.

High-Q model rationale

Seismology data → density/viscosity profile → 1-layer mantle convection Radiogenic heat : ~25 TW

High-Q model rejection indicates the need to modify the mantle density/viscosity profile or geodynamical modeling of mantle convection.

The KamLAND data favor Low-Q, Middle-Q model.

This result suggests mantle multi-layer convection.

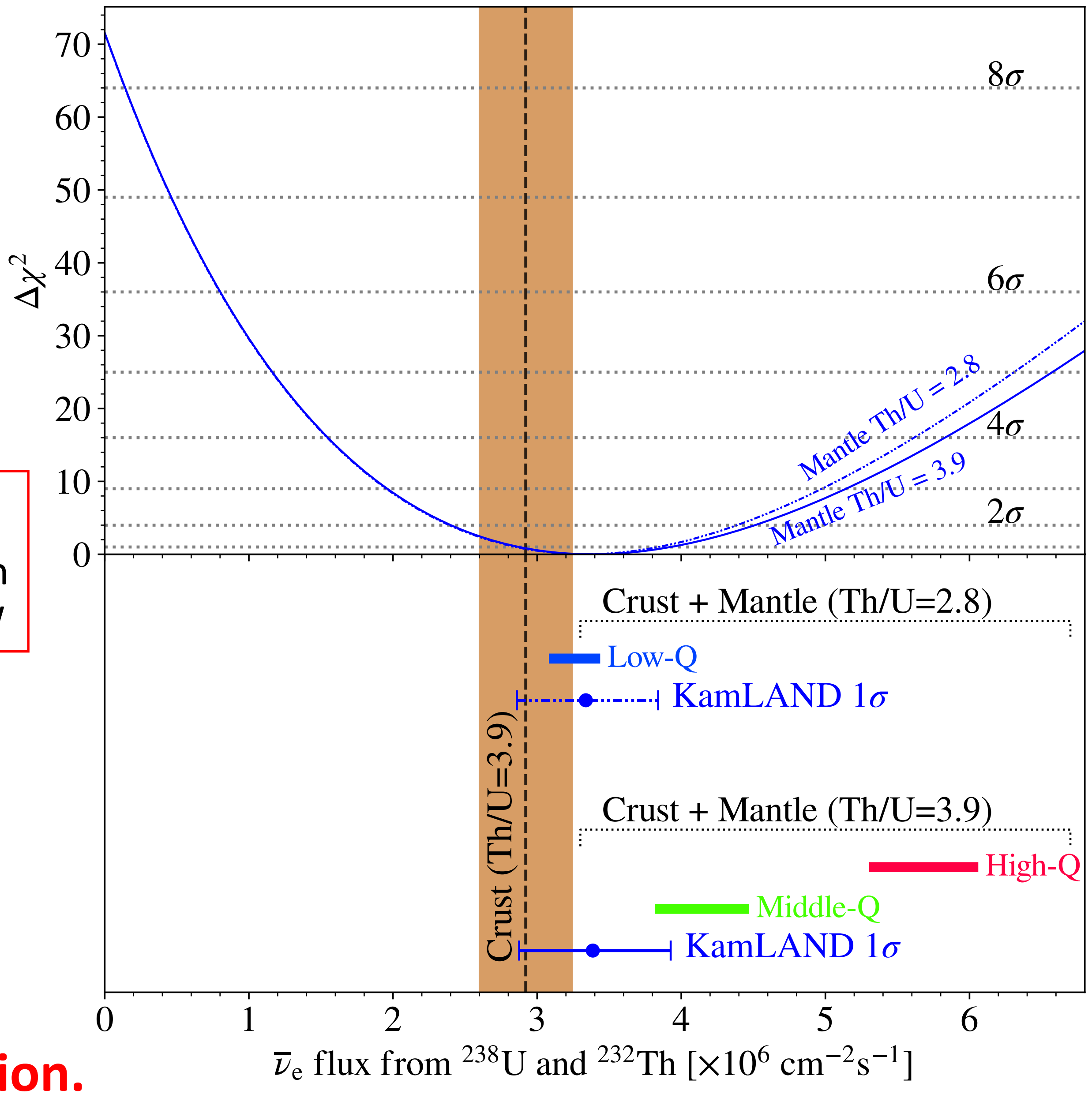

Summary

- The KamLAND experiment has been measuring geoneutrinos from uranium and thorium.
- The reactor-off period in Japan supressed the reactor neutrino background significantly and enabled a spectropic measurement of geoneutrinos from uranium and thorium.

Flux

	$N_{U/Th}$ [event]	flux [$\times 10^5$ cm^{-2}s^{-1}]	flux [TNU]	0-signal rejection
U	$116.6^{+41.0}_{-38.5}$	$14.7^{+5.2}_{-4.8}$	$19.1^{+6.7}_{-6.3}$	3.343σ
Th	$57.5^{+24.5}_{-24.1}$	$23.9^{+10.2}_{-10.0}$	$9.7^{+4.1}_{-4.1}$	2.386σ
U + Th	$173.7^{+29.2}_{-27.7}$	$32.1^{+5.8}_{-5.3}$	$28.6^{+5.1}_{-4.8}$	8.3σ

Radiogenic heat

$$Q^{\mathrm{U}} = 3.3^{+3.2}_{-0.8}\ \mathrm{TW}$$
$$Q^{\mathrm{Th}} = 12.1^{+8.3}_{-8.6}\ \mathrm{TW}$$
$$Q^{\mathrm{U}} + Q^{\mathrm{Th}} = 15.4^{+8.3}_{-7.9}\ \mathrm{TW}$$

Convective Uray ratio = $0.13^{+0.15}_{-0.06}$

- The KamLAND data is consistent with Low-Q and Middle-Q models based on chondrites compositional analysis, whereas the High-Q model is disfavored at 99.76% confidence level with assuming the homogeneous mantle composition, implying multi-layer mantle convection.

Latest publication from KamLAND

ADVANCING EARTH AND SPACE SCIENCE

Geophysical Research Letters®

RESEARCH LETTER
10.1029/2022GL099566

Abundances of Uranium and Thorium Elements in Earth Estimated by Geoneutrino Spectroscopy

S. Abe[1], S. Asami[1], M. Eizuka[1], S. Futagi[1], A. Gando[1], Y. Gando[1,2], T. Gima[1], A. Goto[1], T. Hachiya[1], K. Hata[1], K. Hosokawa[1,3], K. Ichimura[1], S. Ieki[1], H. Ikeda[1], K. Inoue[1], K. Ishidoshiro[1], Y. Kamei[1], N. Kawada[1], Y. Kishimoto[1,4], M. Koga[1,4], M. Kurasawa[1], N. Maemura[1], T. Mitsui[1], H. Miyake[1], T. Nakahata[1], K. Nakamura[1], K. Nakamura[1,4,5], R. Nakamura[1], H. Ozaki[1,6], T. Sakai[1], H. Sambonsugi[1], I. Shimizu[1], Y. Shirahata[1], J. Shirai[1], K. Shiraishi[1], A. Suzuki[1], Y. Suzuki[1], A. Takeuchi[1], K. Tamae[1], H. Watanabe[1], Y. Yoshida[1], S. Obara[7,8], A. K. Ichikawa[9], S. Yoshida[10], S. Umehara[11], K. Fushimi[12], K. Kotera[12], Y. Urano[12], B. E. Berger[4,13], B. K. Fujikawa[4,13], J. G. Learned[14], J. Maricic[14], S. N. Axani[15], Z. Fu[15], J. Smolsky[15], L. A. Winslow[15], Y. Efremenko[4,16], H. J. Karwowski[17,18], D. M. Markoff[17,19], W. Tornow[4,17,20], A. Li[18], J. A. Detwiler[4,21], S. Enomoto[4,21], M. P. Decowski[4,22], C. Grant[23], H. Song[23], T. O'Donnell[24], S. Dell'Oro[24], and (The KamLAND Collaboration)

[1]Research Center for Neutrino Science, Tohoku University, Sendai, Japan, [2]Department of Human Science, Obihiro University of Agriculture and Veterinary Medicine, Obihiro, Japan, [3]Kamioka Observatory, Institute for Cosmic Ray Research, The University of Tokyo, Hida, Japan, [4]Institute for the Physics and Mathematics of the Universe, The University of Tokyo, Kashiwa, Japan, [5]Faculty of Health Sciences, Butsuryo College of Osaka, Osaka, Japan, [6]Graduate Program on Physics for the Universe, Tohoku University, Sendai, Japan, [7]Frontier Research Institute for Interdisciplinary Sciences, Tohoku University, Sendai, Japan, [8]National Institutes for Quantum Science and Technology (QST), Sendai, Japan, [9]Department of Physics, Tohoku University, Sendai, Japan, [10]Graduate School of Science, Osaka University, Osaka, Japan, [11]Research Center for Nuclear Physics (RCNP), Osaka University, Osaka, Japan, [12]Graduate School of Advanced Technology and Science, Tokushima University, Tokushima, Japan, [13]Nuclear Science Division, Lawrence Berkeley National Laboratory, Berkeley, CA, USA, [14]Department of Physics and Astronomy, University of Hawaii at Manoa, Honolulu, HI, USA, [15]Massachusetts Institute of Technology, Cambridge, MA, USA, [16]Department of Physics and Astronomy, University of Tennessee, Knoxville, TN, USA, [17]Triangle Universities Nuclear Laboratory, Durham, NC, USA, [18]The University of North Carolina at Chapel Hill, Chapel Hill, NC, USA, [19]North Carolina Central University, Durham, NC, USA, [20]Physics

Key Points:

- Geoneutrino measurement with low reactor neutrino backgrounds improves the distinct spectroscopic contributions of U and Th
- Radiogenic power in the Earth estimated from this geoneutrino measurement is consistent with a range of models and disfavors the higher power model
- Identifying the Earth's mantle contribution to the total geoneutrino flux strongly depends on an accurate estimation of the crustal contribution

Correspondence to:
N. Kawada,
kawada@awa.tohoku.ac.jp

Citation:
Abe, S., Asami, S., Eizuka, M., Futagi, S., Gando, A., Gando, Y., et al. (2022). Abundances of uranium and thorium elements in Earth estimated by geoneutrino spectroscopy. *Geophysical Research Letters*, *49*, e2022GL099566. https://doi.org/10.1029/2022GL099566

https://agupubs.onlinelibrary.wiley.com/doi/10.1029/2022GL099566

Geophysical Research Letters, Volume 49, Issue 16, e2022GL099566

First published on 2022/Aug./11

<u>Please check it !!</u>

Eos *Science News by AGU*

ABOUT | SPECIAL REPORTS | TOPICS | PROJECTS | NEWSLETTER | SUBMIT TO *EOS*

Estimating Uranium and Thorium Abundance with Geoneutrinos

Terrestrial electron antineutrino observations provide new constraints on the contributions of radiogenic heat in the mantle.

By Morgan Rehnberg 31 August 2022

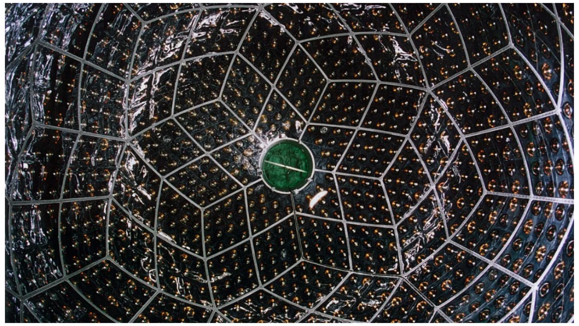

The KamLAND detector, above, can detect electron antineutrinos produced through the decay of uranium and thorium deep inside Earth when they collide with the atomic nuclei. Credit: Research Center for Neutrino Science, Tohoku University

The editors of GRL have selected our paper to be featuread as "Research Spotlight" on Eos.org !!

(144 papers in July from GRL, 1 Research Spotlight)

AGU Research Spotlights summarize the research and findings of the best accepted articles for the broad Earth and space science community. Research Spotlights also may be sent to interested news media and may appear in the monthly *Eos* print version in addition to being published on Eos.org.

https://eos.org/research-spotlights/estimating-uranium-and-thorium-abundance-with-geoneutrinos

Backup slides

Structural modeling by seismology

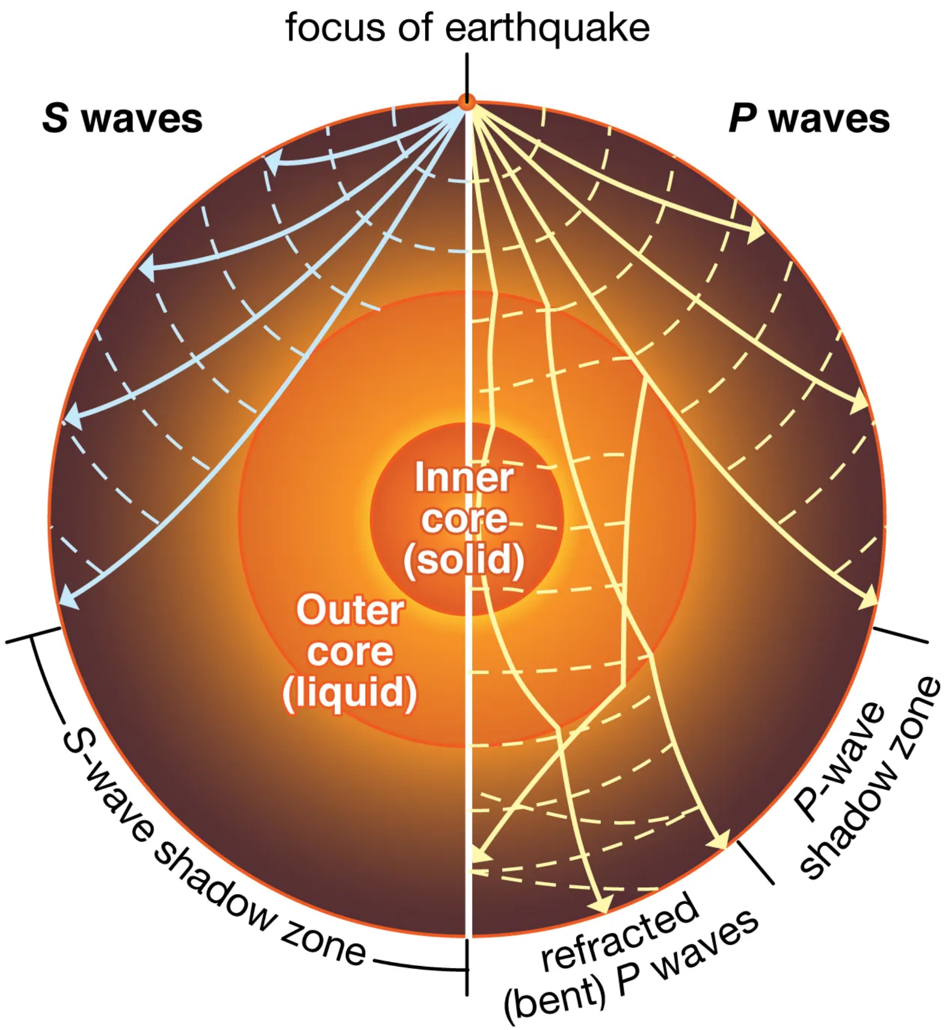

Multi-point observation of earthquakes propagating through the Earth

- Density and viscosity profiles of deep earth
  Multi layer of core–mantle–crust
- **No compositional information**

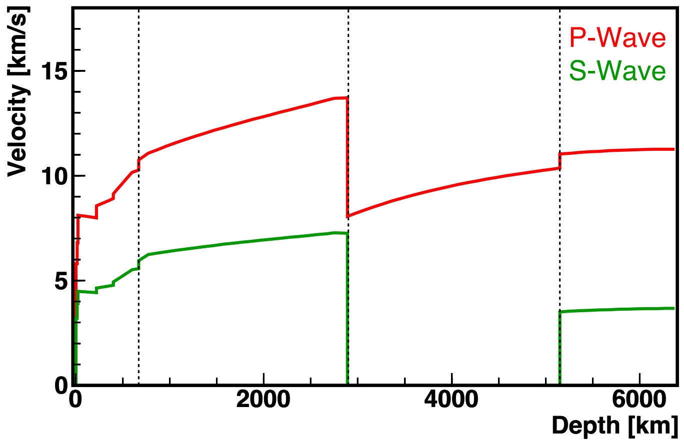

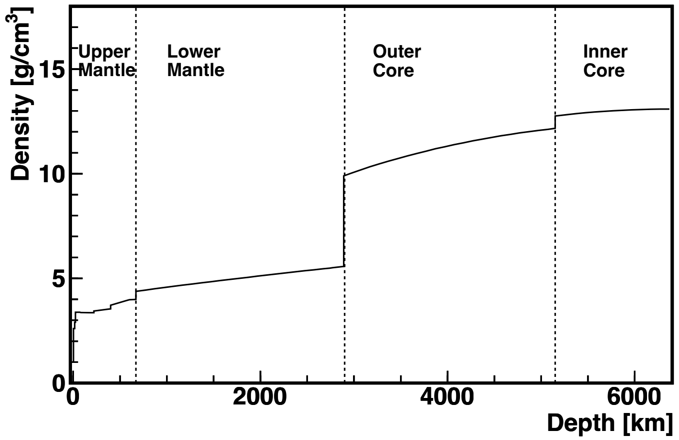

Compositional modeling by geo(cosmo)chemistry

CI carbonaceous chondrite

Enstatite chondrite

Earth's chemical composition estimate based on chondrite meteorites and earth samples

Bulk-Silicate Earth (BSE) model give average composition of mantle+crust.

Earth samples give crustal compositional estimation.

The mantle composition is estimated by subtracting crustal elements from the BSE composition.

Candidate material of the Earth : chondrites

CI carbonaceous chondrite :
- compositional similarity to solar atmosphere
- abundant volatile elements

Enstatite chondrite :
- isotopic similarity to the Earth
- abundant iron

We do never know which chondrite formed the Earth.
There be never direct sampling of deep earth.

→ Direct verification is needed.

Geoneutrino flux estimate

Flux estimate

The flux at the surface is calculated from knowledges of particle physics and geoscientific parameters.

$$\frac{d\Phi}{dR} = \sum_{i \in U,Th} A_i \cdot N_i \int_{earth} d^3\vec{r'} \frac{a_i(\vec{r'})\rho(\vec{r'})}{4\pi|\vec{r}-\vec{r'}|^2} P(|\vec{r}-\vec{r'}|) \cdot \delta(|\vec{r}-\vec{r'}|-R)$$

Decay rate (A_i)

concentration (a_i)

density (ρ)

Neutrino luminosity per decay (N_i)

Survival probability (P)

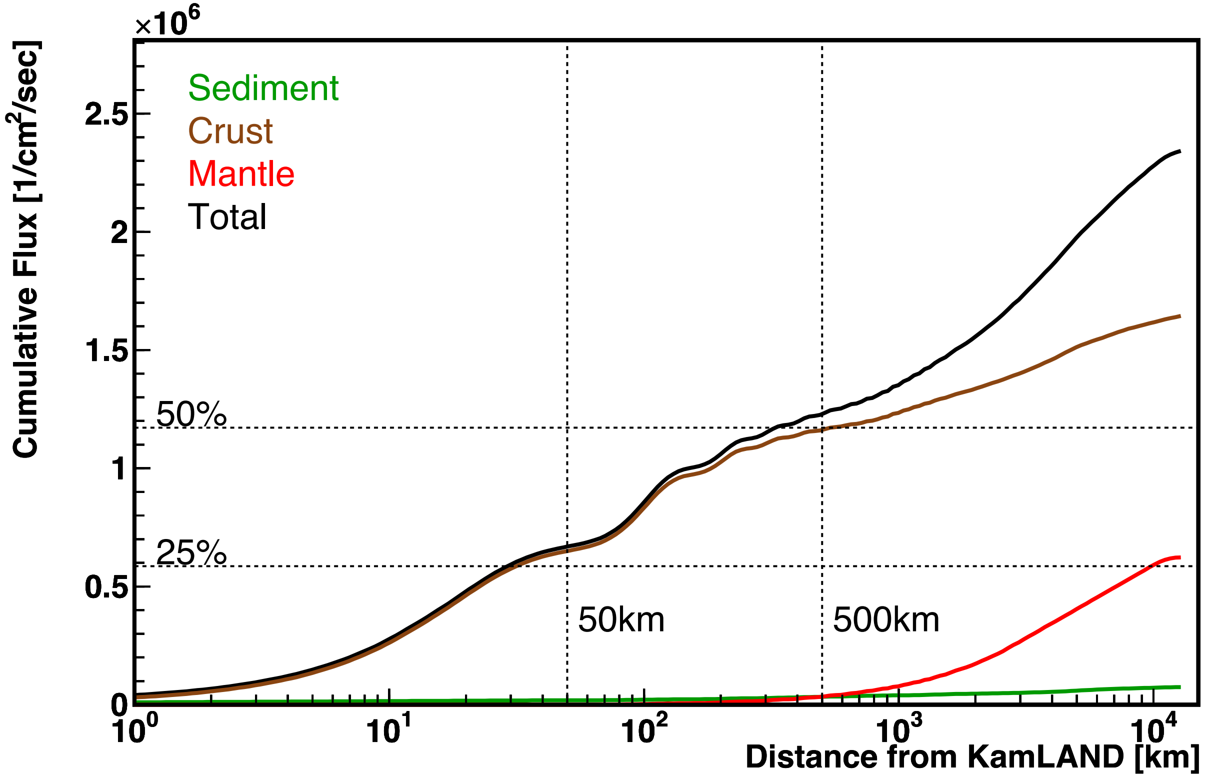

~ 70%

~27%

~ 3%

Our reference estimation (Enotomo et al 2007)

Crust / Sediment

- Based on geo(cosmo)chemical studies
- Local geological effect was averaged.
- The dominant uncertainty came from U,Th concentration measurement.

Mantle

- Subtraction of crust+sediment from BSE compositional model (M&S2003)
- We test this with geoneutrino

Broad science objectives of KamLAND experiment

10^{-1} 10^{0} 10^{1} 10^{2} 10^{3} Neurino energy [MeV]

Solar neutrinos

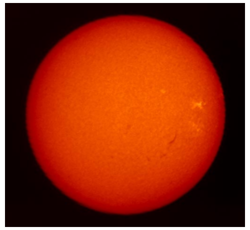

Solar mechanism
Evolution of slars
Neutrino astronomy

Reactor neutrinos

Neutrino oscillation

Nature of neutrinos

Astrophysical burst neutrinos

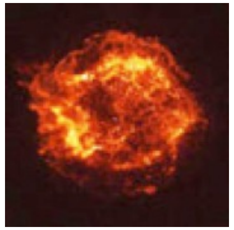

Supernova
GRB
Solar flare etc..

Neutrino astronomy

Accelerater neutrinos

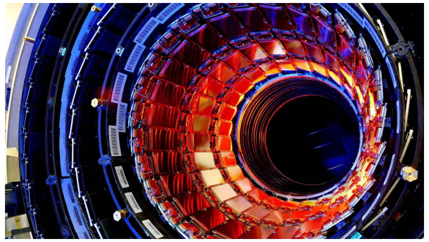

CP violation in
lepton sector

Geoneutrinos

Radioactivity and heat
inside the Earth

Neutrino geoscience

Neutrino provides unique probe of particle physics, astronomy and geoscience.

Geoneutrino measurement in KamLAND

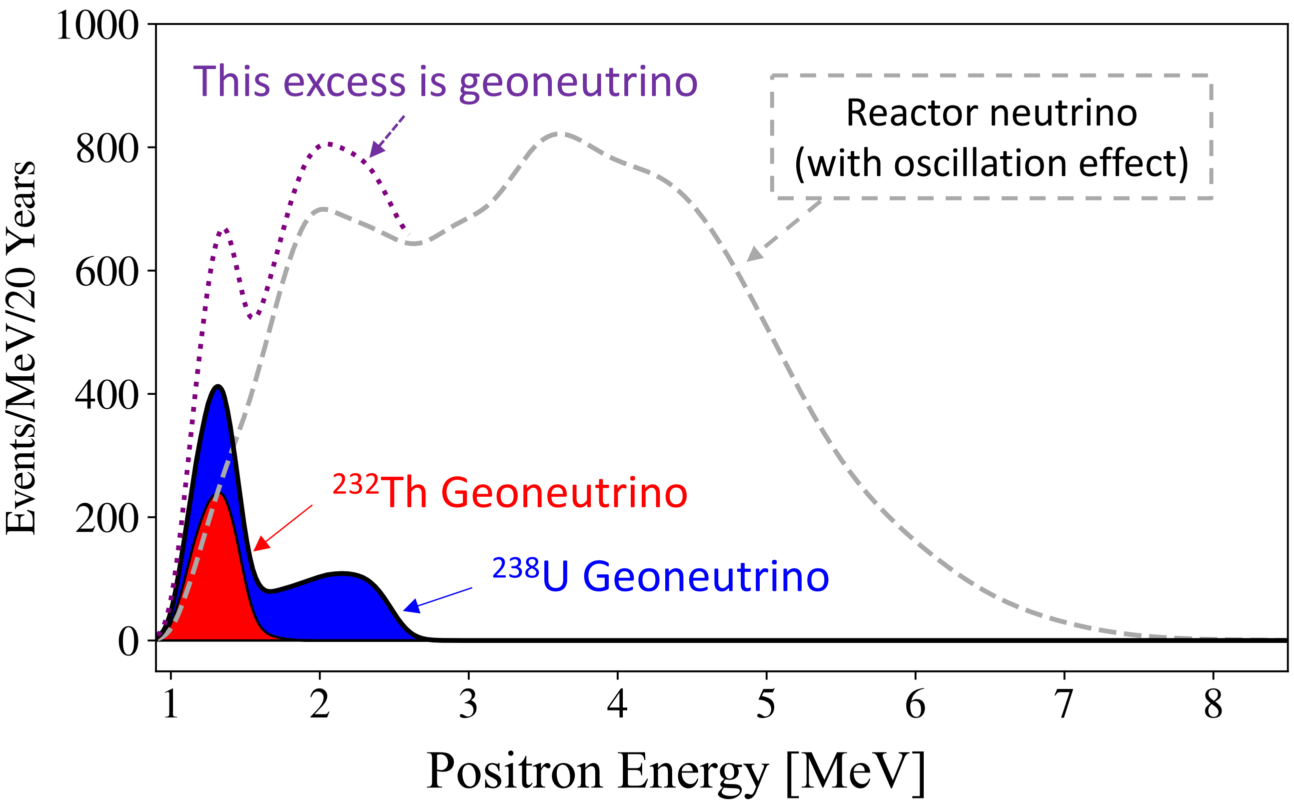

How does KamLAND measure geoneutrinos?

- KamLAND can measure rate and energy of neutrinos.
- Reactor neutrinos are the dominant background due to shared energy range.

- We can distinguish geoneutrinos from other neutrinos statistically by apllying energy (and time) spectrum fitting.

Large statistics and reduction of systematic uncertainties are very important.

It is also important to construct detector away from reactors.

Neutrino oscillation measurement

KamLAND can detect neutrinos from reactors with average distance of 180 km.

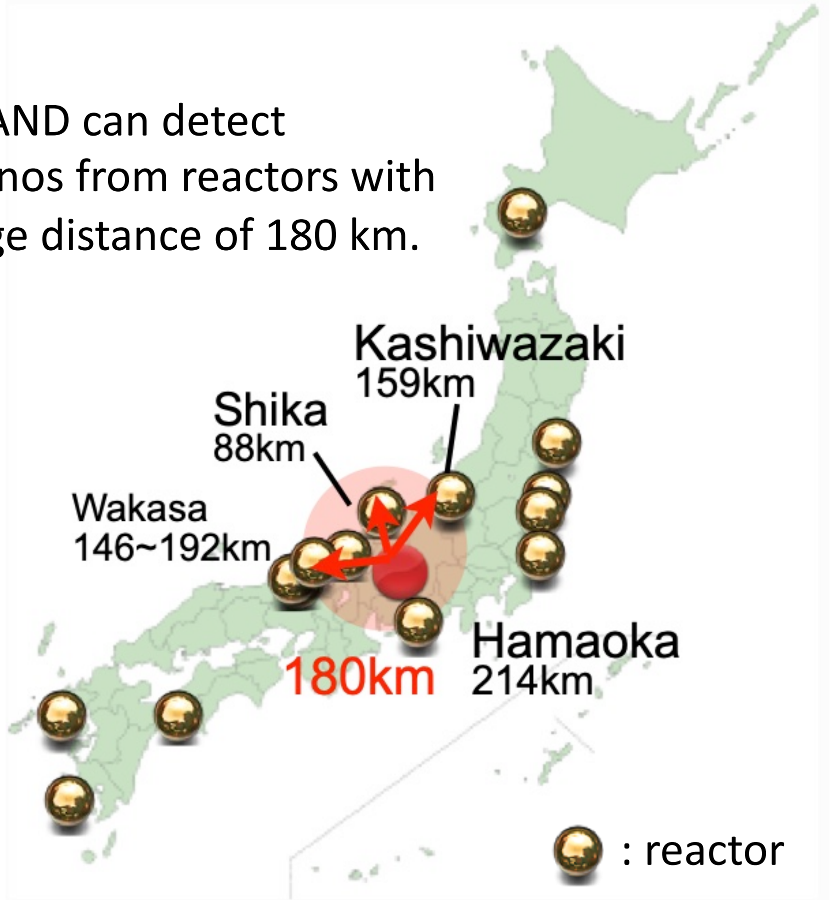

Two-flavor survival probability is appximated as

$$\widetilde{\mathrm{P}}^{2\nu}_{\mathrm{ee}} = 1 - \sin^2\left(2\widetilde{\theta}_{12}\right)\sin^2\left(\frac{\Delta\widetilde{m}^2_{21}L}{E_\nu}\right)$$

$\widetilde{\theta}_{12}, \widetilde{m}_{21}$: ν_1-ν_2 oscillation parameters in earth

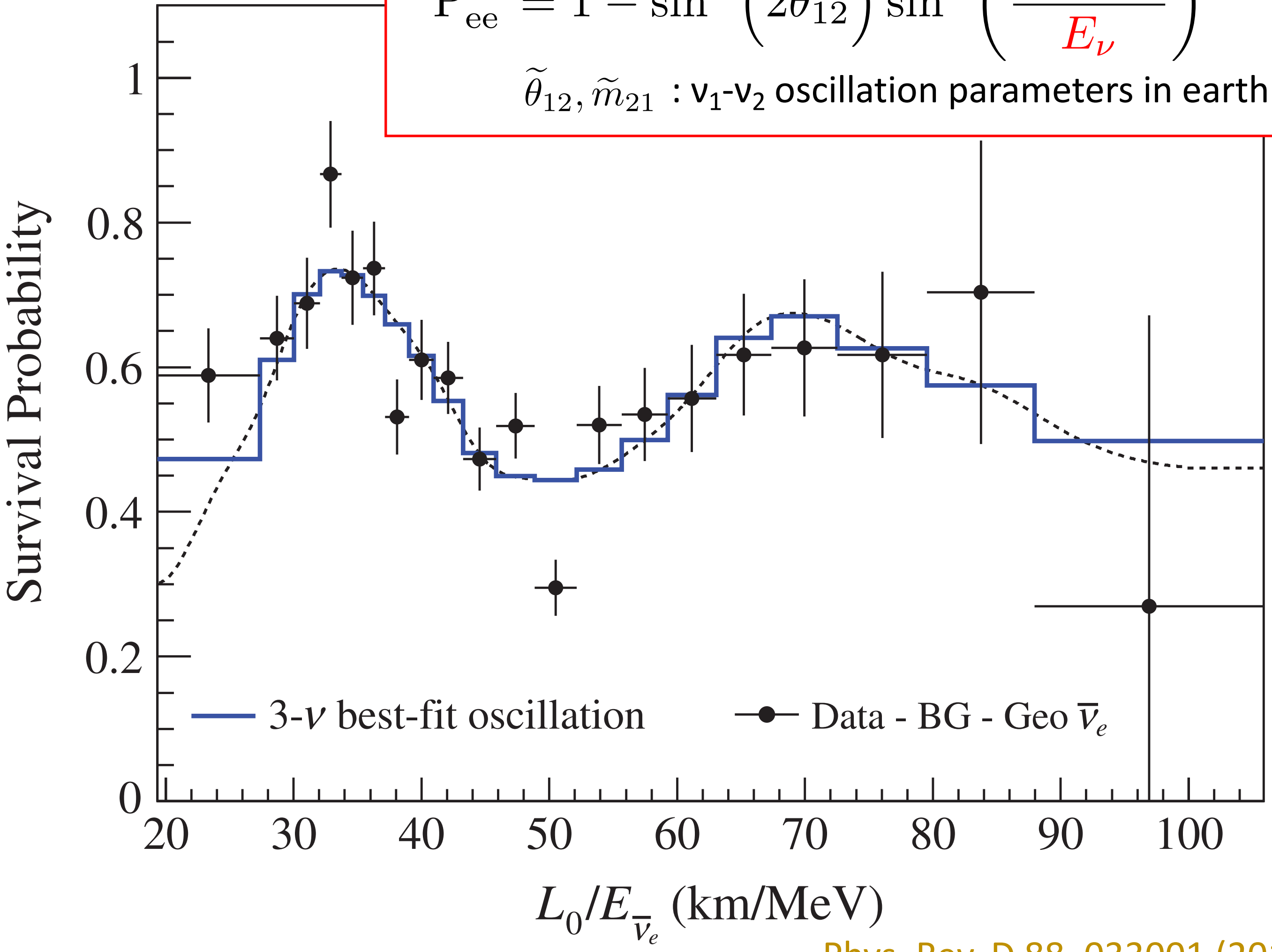

Phys. Rev. D 88, 033001 (2013)

KamLAND measured 2 cycles of neutrino oscillation precisely for the first time in the world.

Liquid scintillator purification with distillation

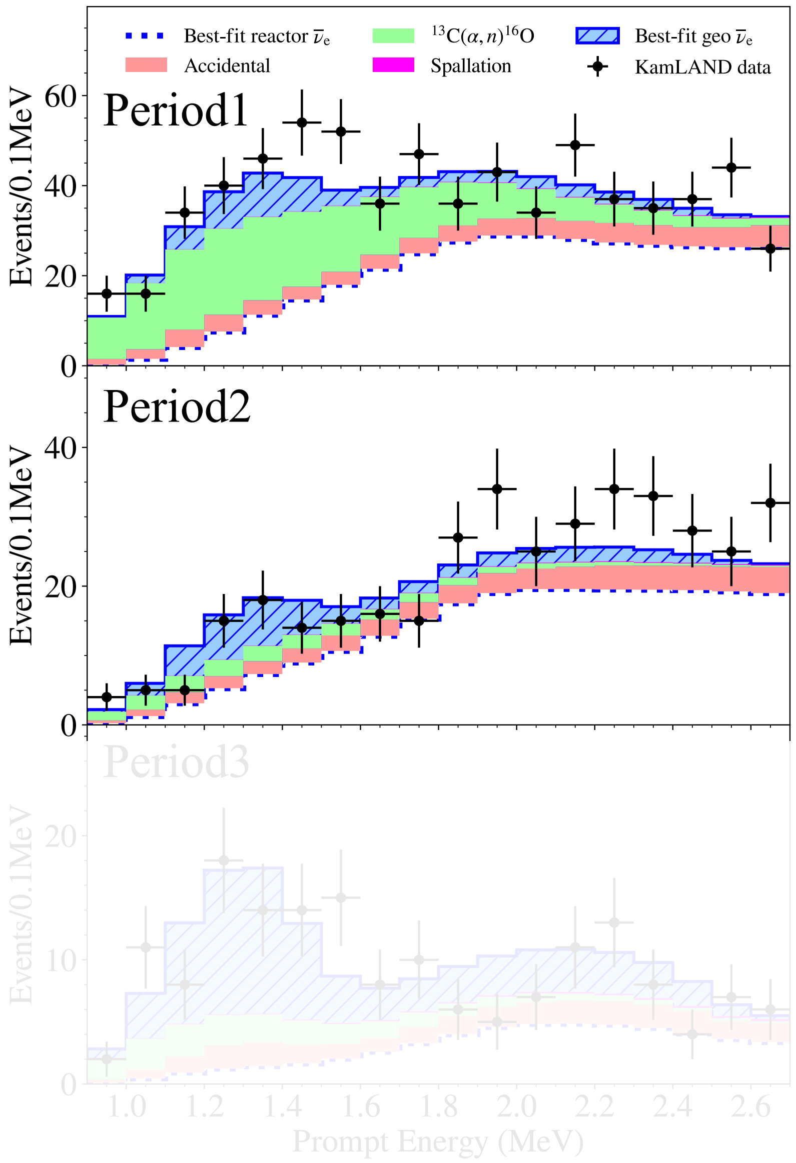

$^{13}C(\alpha, n)^{16*}O$ background

- Mimic neutrino signal
- Triggered by α particle
- Main α source : ^{210}Po
- Main ^{210}Po source : ^{210}Pb

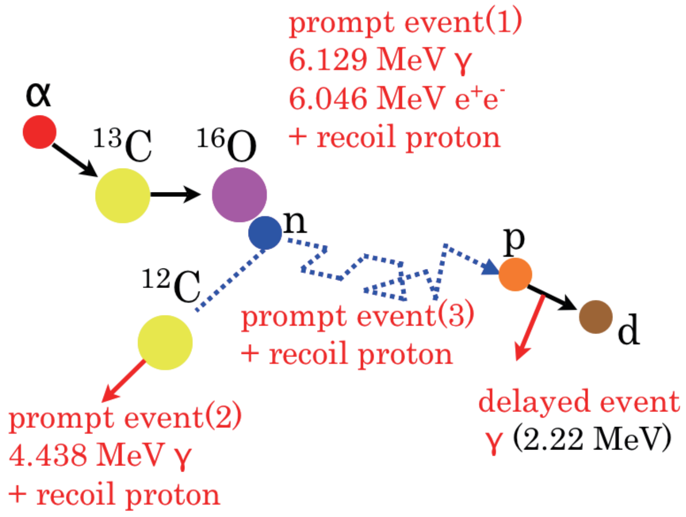

Reduction of ^{210}Pb by distillation campaigns in 2007 and 2008

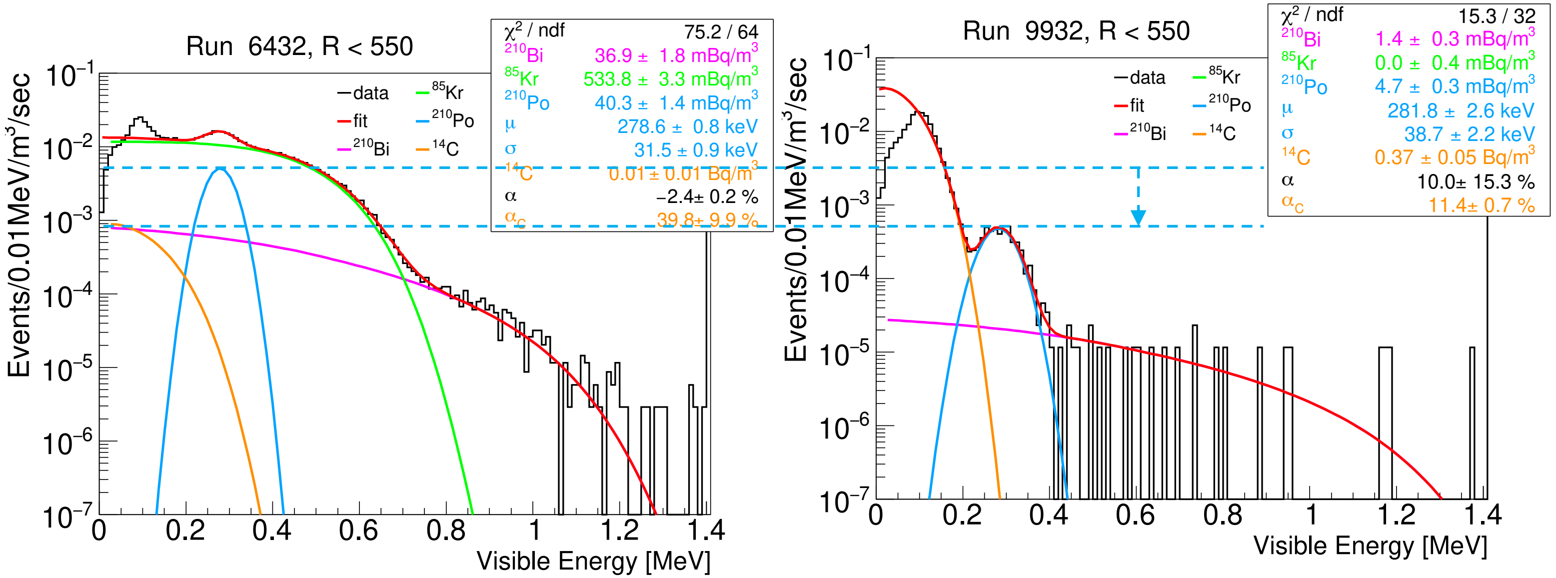

Impact of reactor-off period

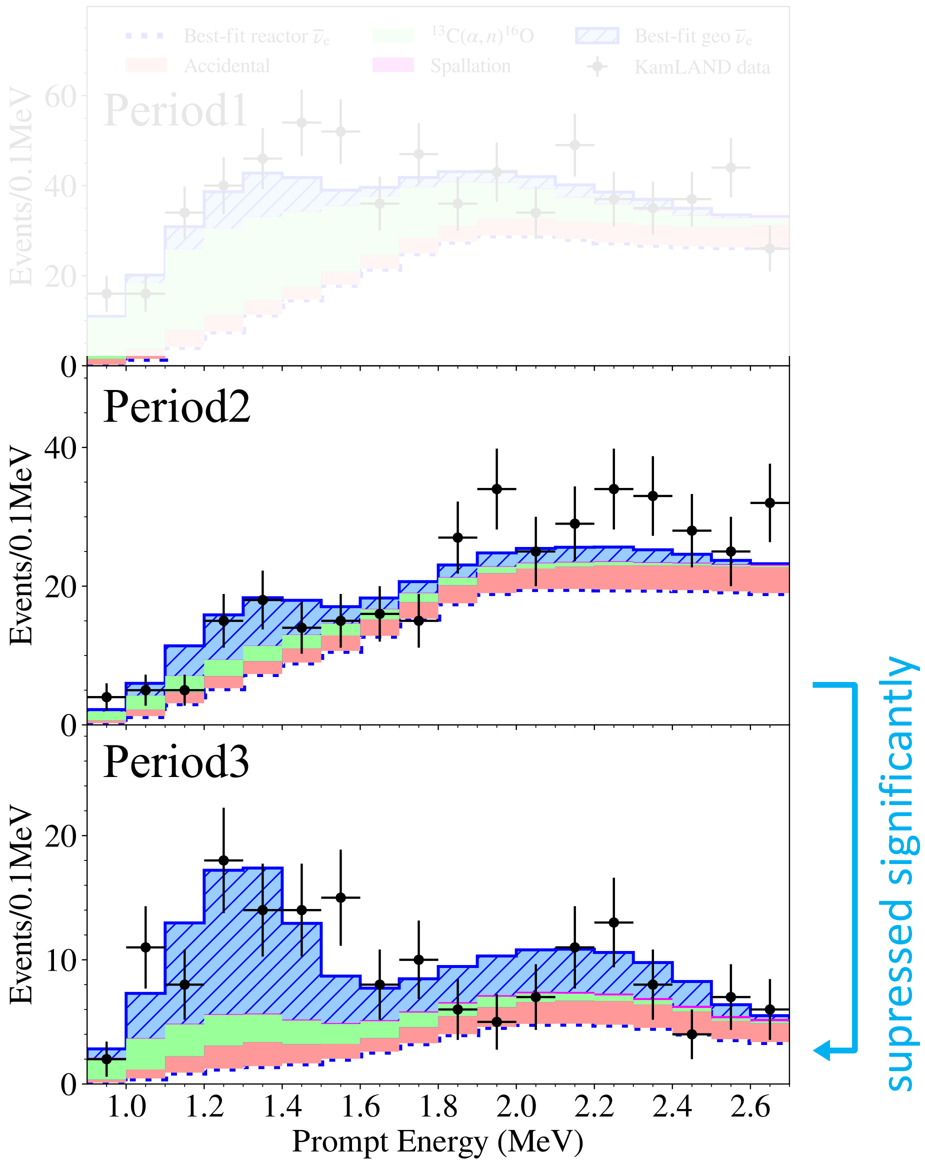

Reactor neutrino background

- Significantly decreased due to the reactor-off environment

Accidental-coincidence background

- Suppressed by optimization of likelihood-based anti-neutrino event selection in reactor-off period.

Geoneutrino signal

- In the reactor-off period, the spectrum shape can be seen clearly.

Statistical power of reactor-off period

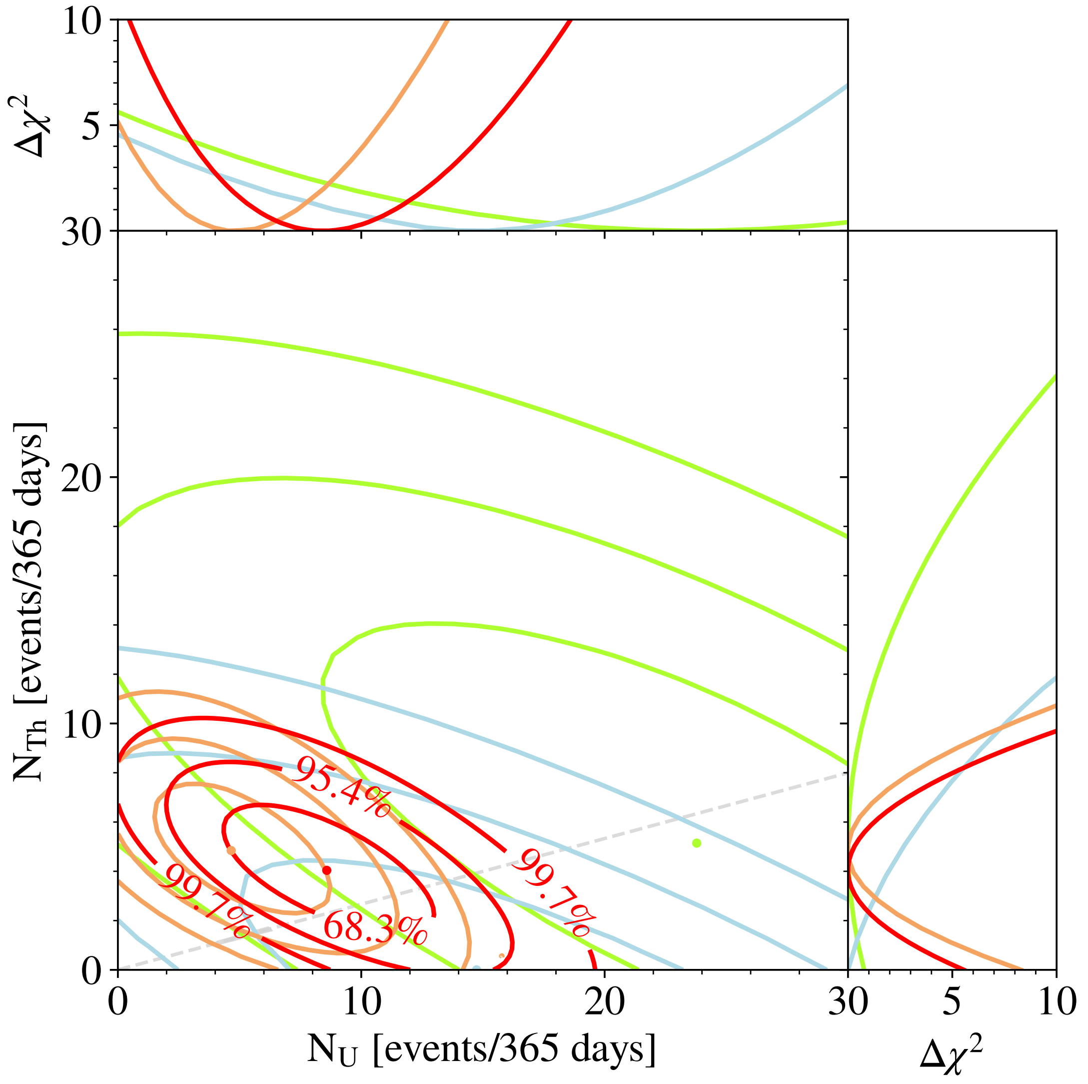

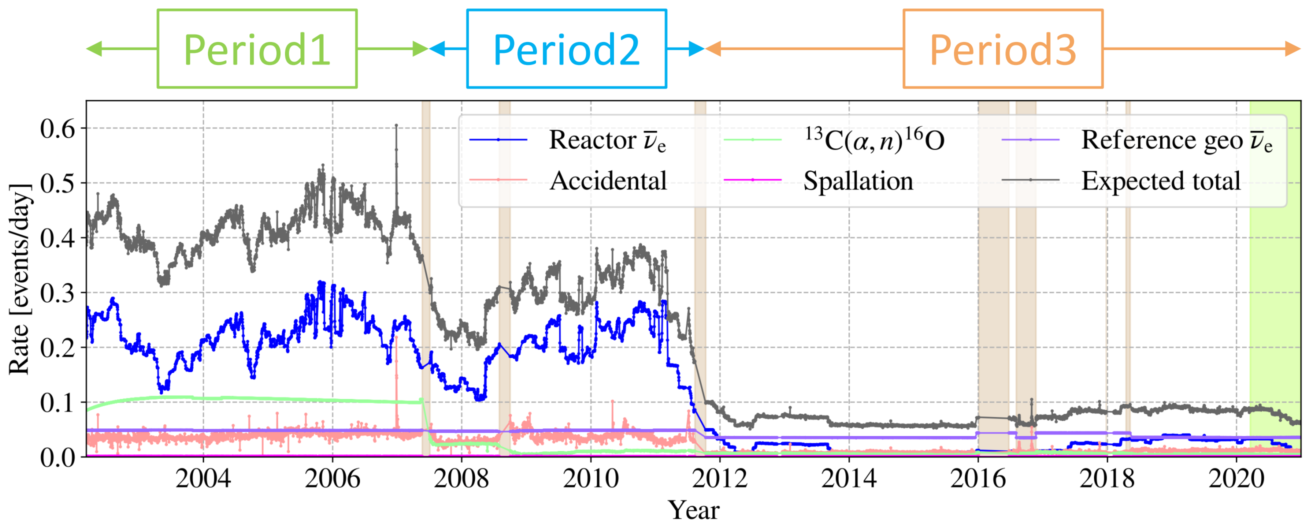

Period3 (reactor-off period) contributes to the determination of geoneutrino flux from Uranium and Thorium.

Anti-neutrino event selection

Delayed-coincidence

Finding spacial and time coincident events

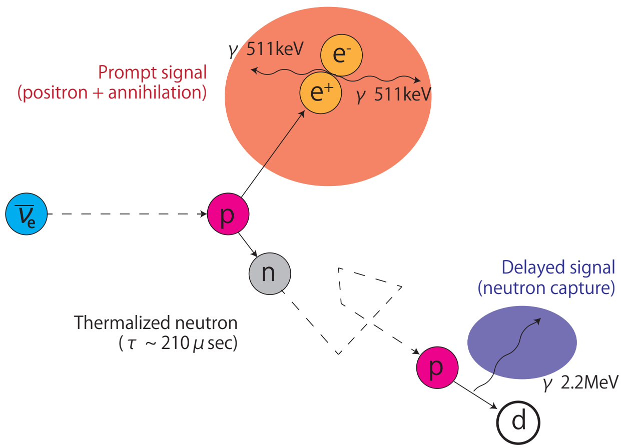

parameter	criteria
prompt energy [MeV]	$0.9 \leq E_{\mathrm{p}} < 8.5$
delayed energy [MeV]	$1.8 \leq E_{\mathrm{d}} < 2.6$ $4.4 \leq E_{\mathrm{d}} < 5.6$
space correlation [m]	$\Delta R < 2.0$
time correlation [μs]	$0.5 \leq \Delta T < 1000$
fiducial volume [m]	$R_{\mathrm{p}} < 6$ & $R_{\mathrm{d}} < 6$

Likelihood selection

$$f_{\overline{\nu}_{\mathrm{e}}} = f_{\overline{\nu}_{\mathrm{e}}}(E_{\mathrm{p}}, E_{\mathrm{d}}, \Delta R, \Delta T, R_{\mathrm{p}}, R_{\mathrm{d}})$$: Signal PDF (Geant4 simulation)

$$f_{\mathrm{accidental}} = f_{\mathrm{accidental}}(E_{\mathrm{p}}, E_{\mathrm{d}}, \Delta R, \Delta T, R_{\mathrm{p}}, R_{\mathrm{d}})$$: Accidental PDF (data driven)

$$\mathcal{L}_{\mathrm{ratio}}(E_{\mathrm{p}}) = \frac{f_{\overline{\nu}_{\mathrm{e}}}}{f_{\overline{\nu}_{\mathrm{e}}} + f_{\mathrm{accidental}}}$$: Likelihood ratio;
The probability that an DC pair is a IBD reaction

Anti-neutrino event selection

Likelihood selection threshold

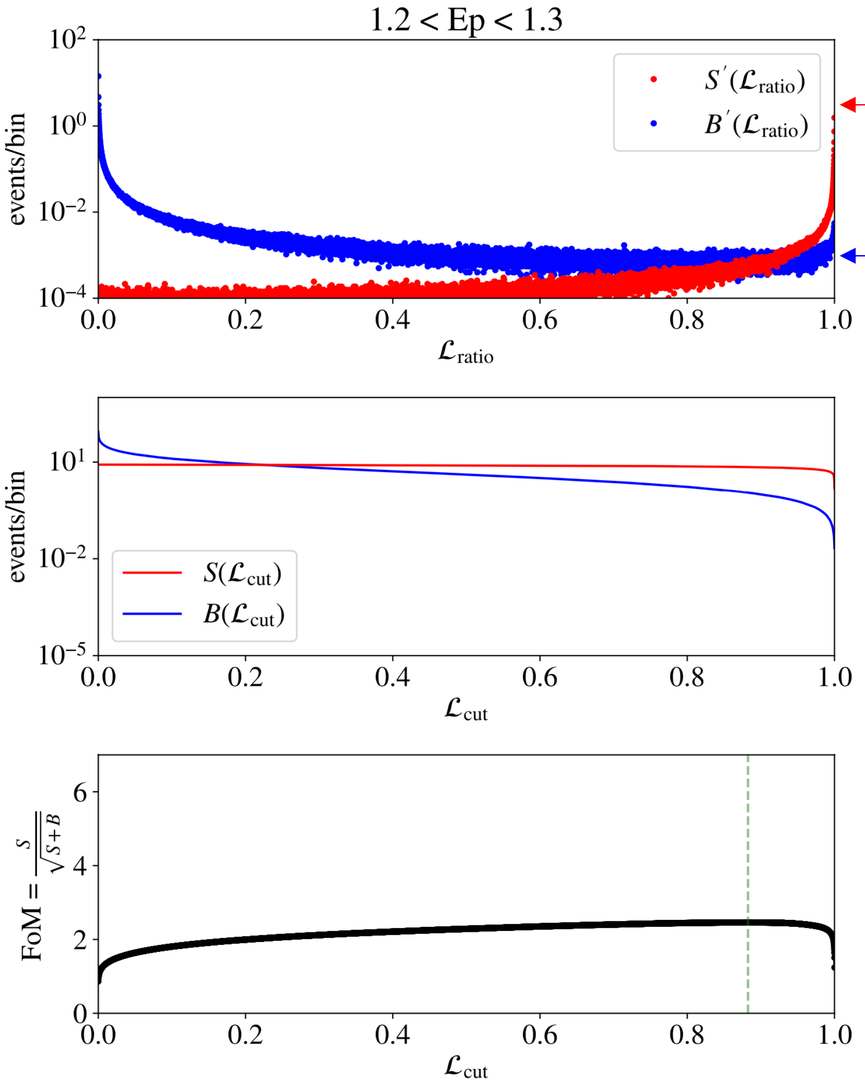

Geant4-simulate $\mathcal{L}_{\mathrm{ratio}}$ distribution in IBD

Data-driven $\mathcal{L}_{\mathrm{ratio}}$ distribution in accidental-coincidence

Right-side integral of $\mathcal{L}_{\mathrm{ratio}}$ = Remaining events if we apply a cut $\mathcal{L}_{\mathrm{ratio}} > \mathcal{L}_{\mathrm{cut}}$

$$\mathrm{FoM}(\mathcal{L}_{\mathrm{cut}}) = \frac{S(\mathcal{L}_{\mathrm{cut}})}{S(\mathcal{L}_{\mathrm{cut}}) + B(\mathcal{L}_{\mathrm{cut}})}$$

The best $\mathcal{L}_{\mathrm{cut}}$ maximize this FoM.

Accidental-coincidence background

Only delayed-coincidence

parameter	criteria
prompt energy [MeV]	$0.9 \leq E_p < 8.5$
delayed energy [MeV]	$1.8 \leq E_d < 2.6$ $4.4 \leq E_d < 5.6$
space correlation [m]	$\Delta R < 2.0$
time correlation [μs]	~~$0.5 \leq \Delta T < 1000$~~
fiducial volume [m]	$R_p < 6$ & $R_d < 6$

0.2–1.2 [sec]

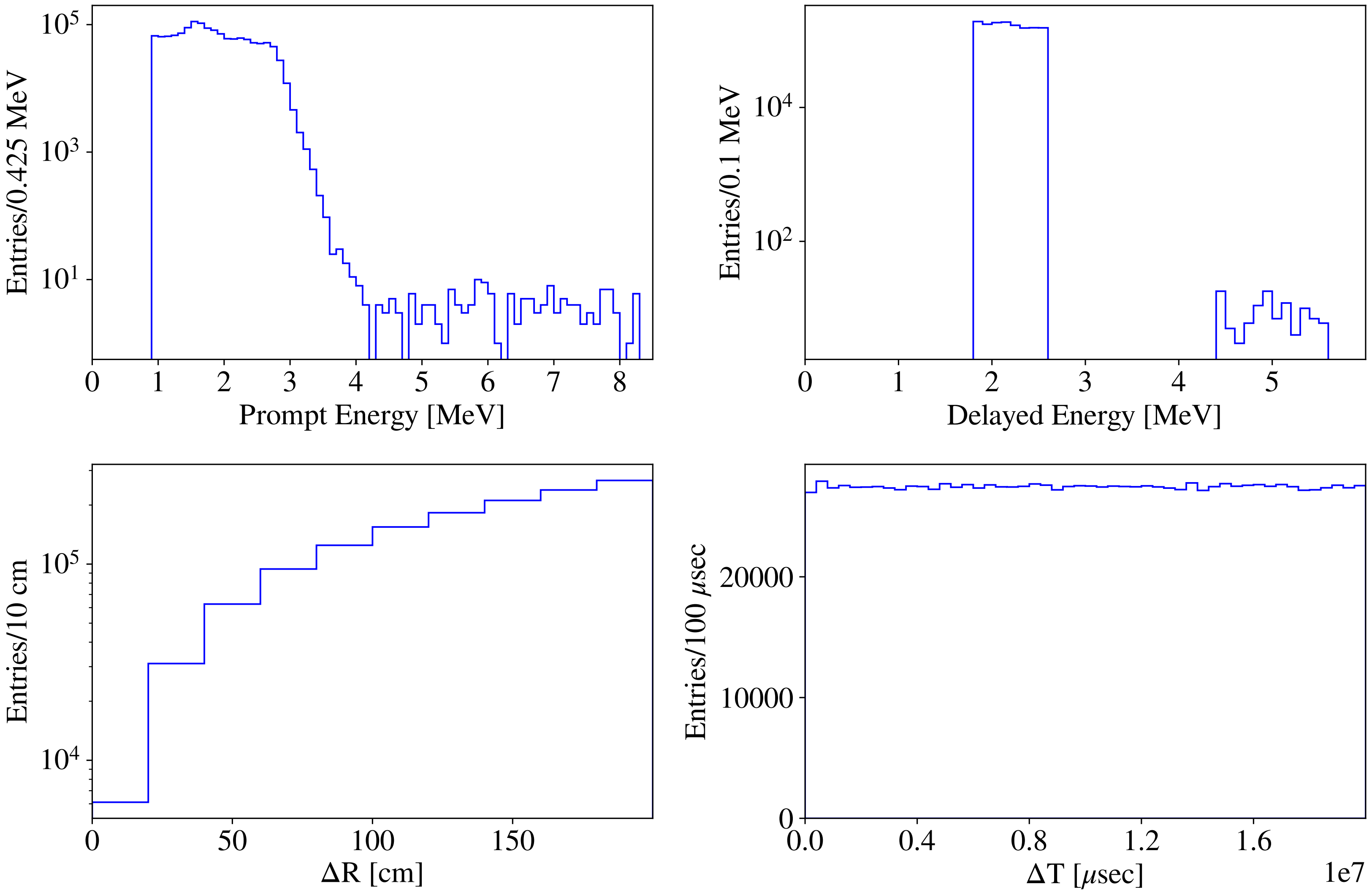

Accidental-coincidence background

Delayed-coincidence only

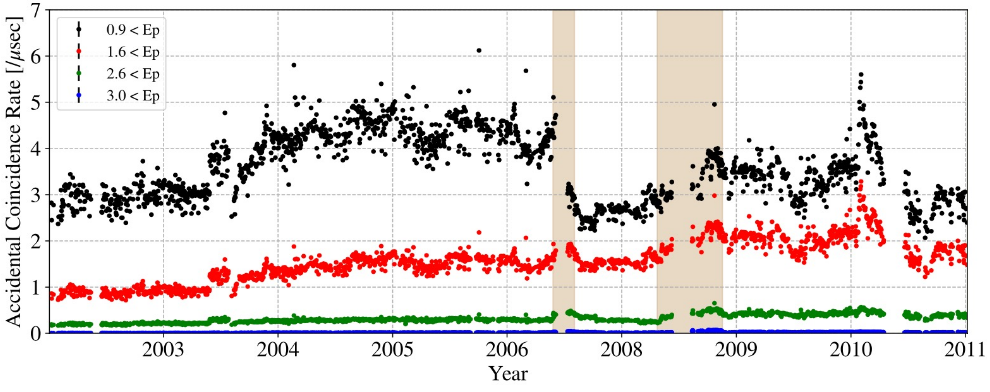

Figure 5.16: Time variation of the accidental coincidence rate in Period1 and Period2. The accidental coincidence events are selected by the delayed-coincidence method and the likelihood selection has not been applied.

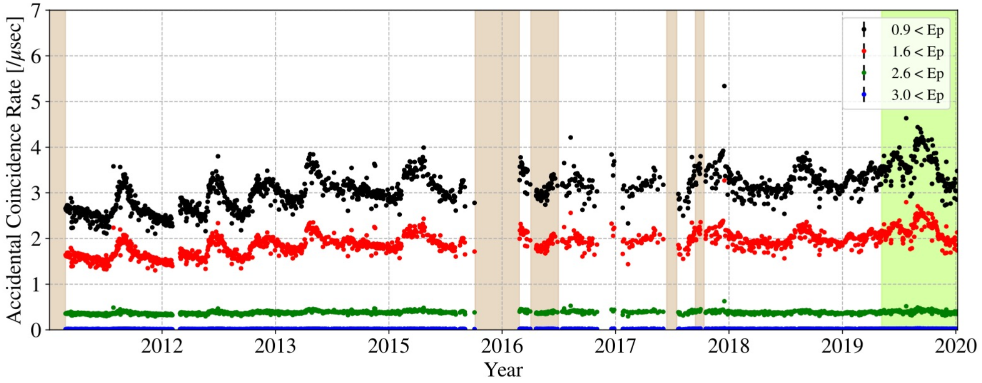

Figure 5.17: Time variation of the accidental coincidence rate in Period3. The accidental coincidence events are selected by the delayed-coincidence method and the likelihood selection has not been applied.

Likelihood selection applied

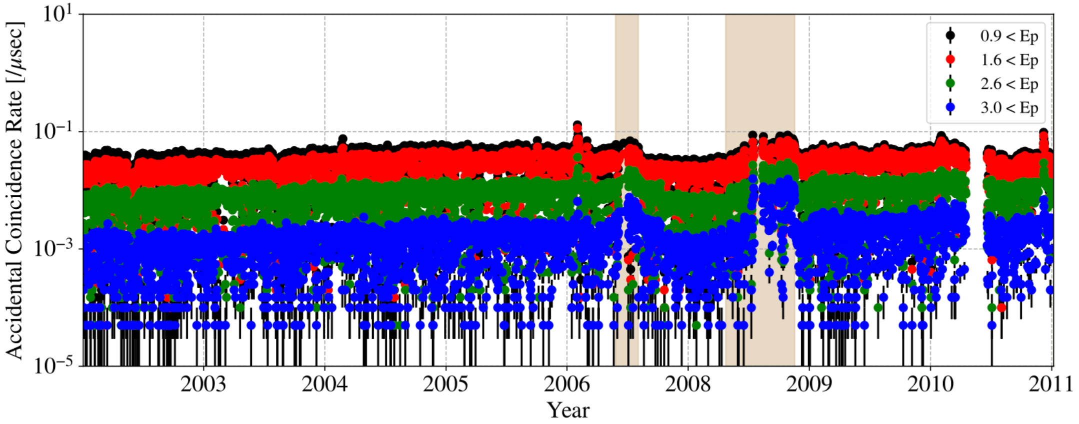

Figure 6.43: Time variation of the accidental coincidence background rate after Likelihood cut in Period1 and Period2.

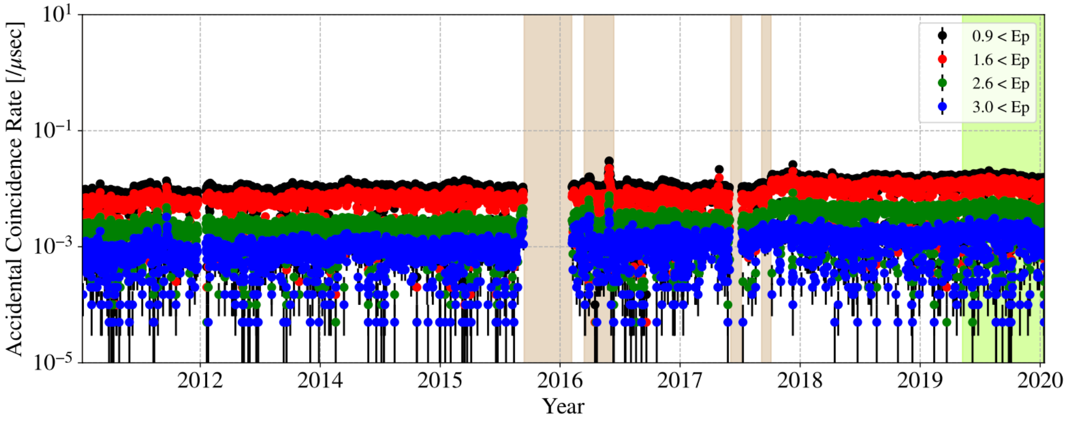

Figure 6.44: Time variation of the accidental coincidence background rate after Likelihood cut in Period3

Why acci. BG was suppressed in period3 ?

‘02/Mar./9–’03/Oct./31 (period1)

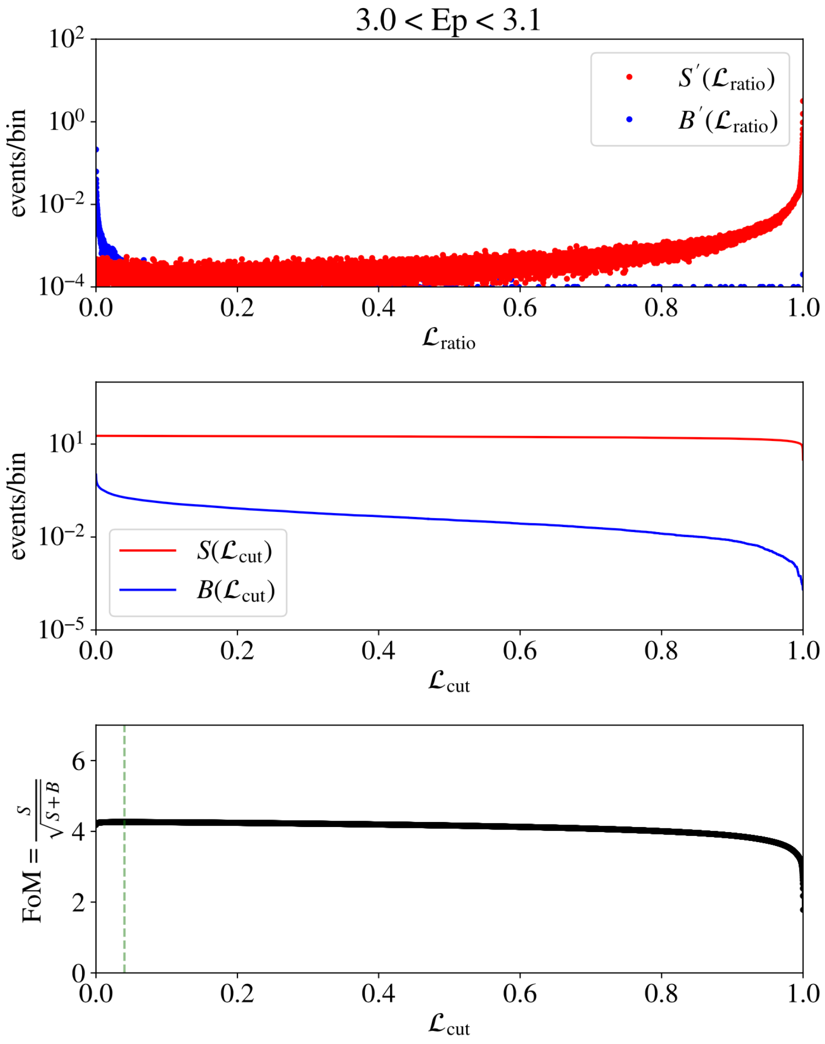

Figure 5.20: Likelihood selection procedure for $3.0 < E_p < 3.5$ in LH-0

Fewer IBD expectation in reactor-off period

Accidental coincidence rate does not change in reactor-off period

The optimized threshold shifted to right.

Higher threshold suppressed more accidental background.

‘18/May/19—’20/Dec./31 (Period3)

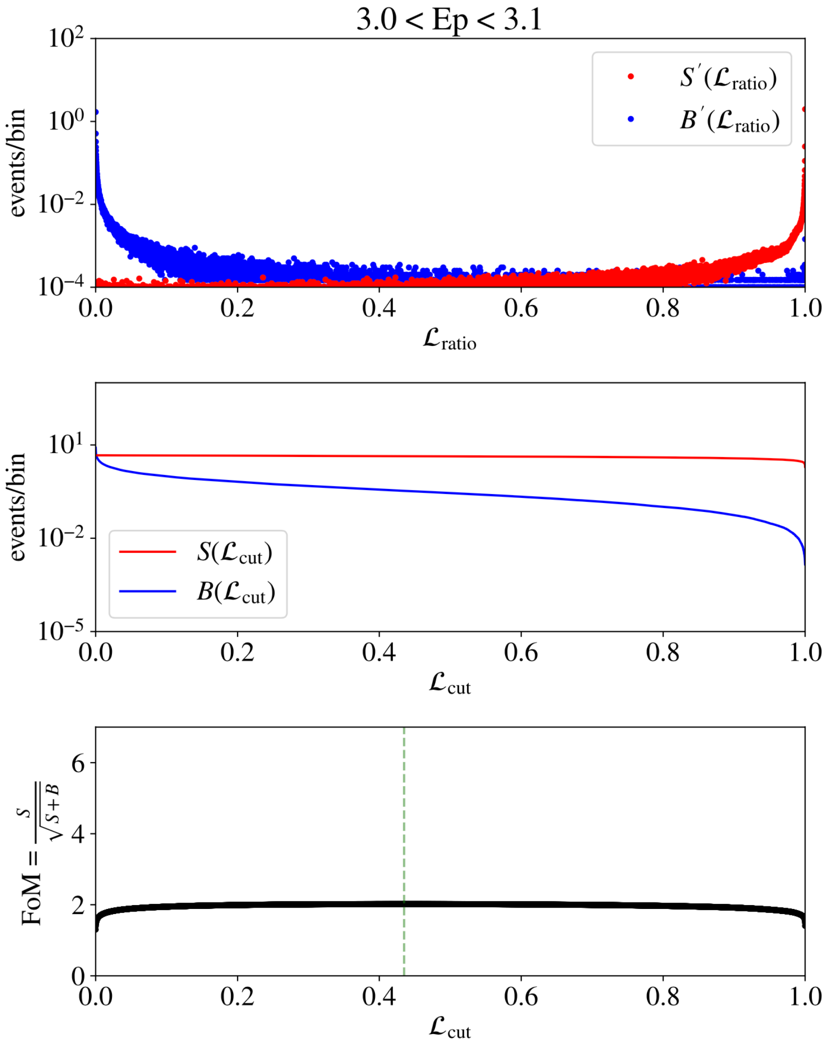

Figure 5.23: Likelihood selection procedure for $3.0 < E_p < 3.5$ in LH-7

Reactor neutrino spectrum

Neutrino spectrum from a reactor

IBD cross section

$$S(E_\nu) = S_{\mathrm{DB}}(E_\nu) + \sum_{x \in \mathrm{isotope}} (f_i^x - f_{\mathrm{DB}}^x) S_{\mathrm{HM}}^x(E_\nu) \sigma_{\mathrm{IBD}}(E_\nu)$$

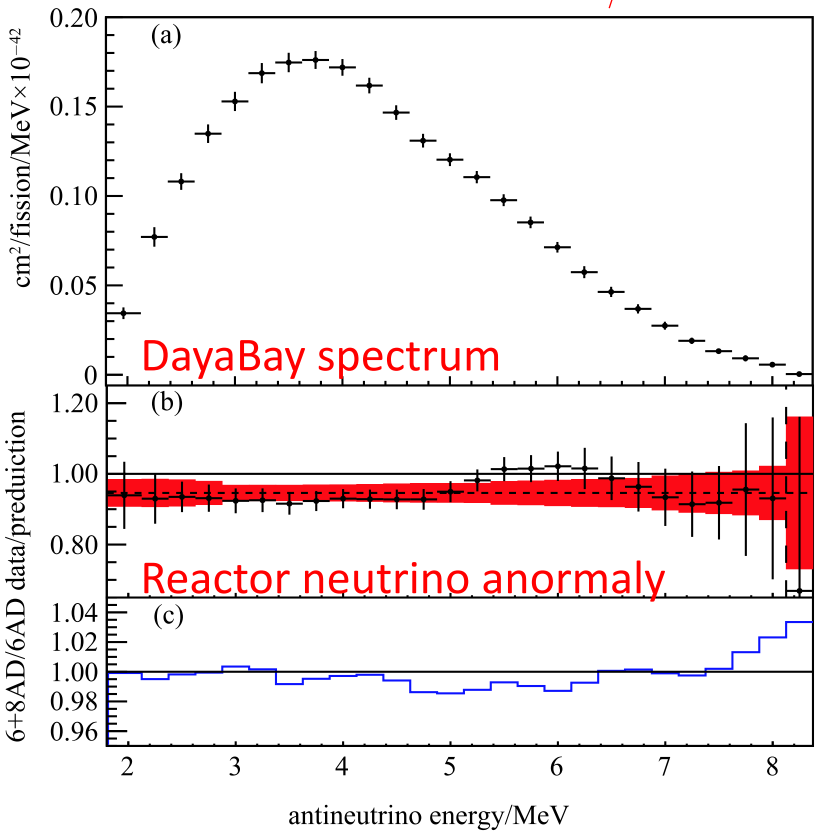

Differences in fission fraction of major isotopes

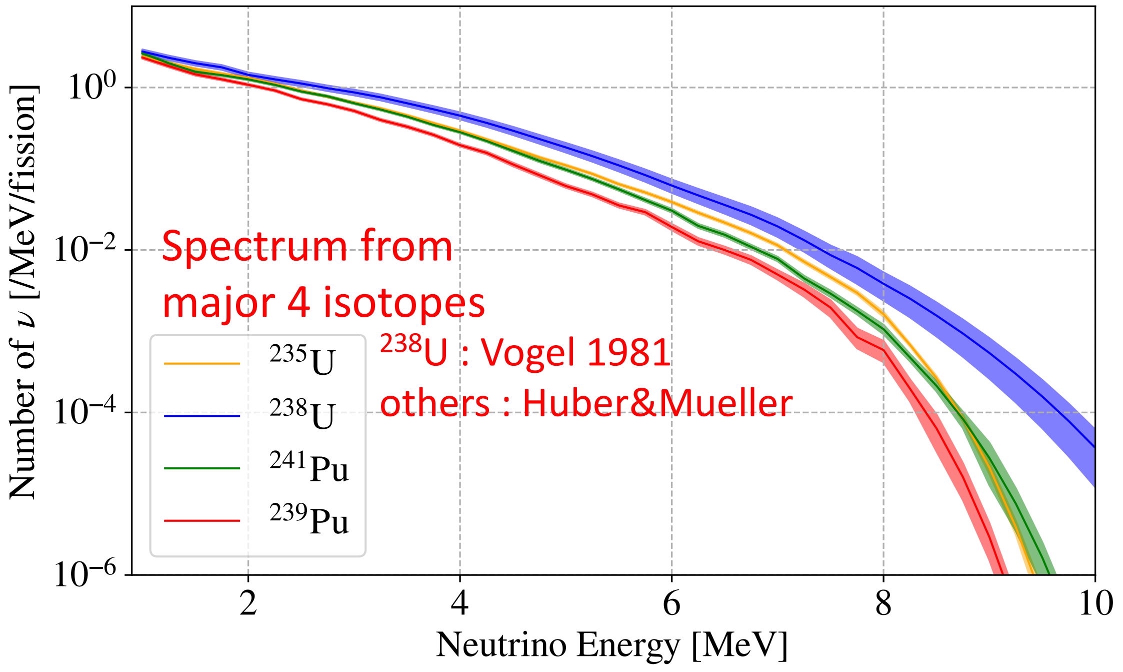

Distillation system in KamLAND site